




Fractional Chern insulator with Rydberg-dressed neutral atoms

Yang Zhao ^{1,2} and Xiao-Feng Shi ³

¹Hebei Normal University, Shijiazhuang, Hebei 050024, China

²Northwestern Polytechnical University, Xi'an 710072, China

³School of Physics, Xidian University, Xi'an 710071, China

 (Received 15 May 2023; revised 28 August 2023; accepted 18 October 2023; published 6 November 2023)

Topological nontrivial bands can be realized via Rydberg-dressed neutral atoms. We propose a two-dimensional hard-core boson model with a topological flat band on a honeycomb array, where the particle hopping is realized via van der Waals interactions that exchange the Rydberg states of two interacting atoms, while nonzero phases associated with hopping arises from the transfer of laser phase to the wave functions of Rydberg atoms. Using exactly diagonalization and infinite density matrix renormalization group simulation, we find in the system a fractional Chern insulator phase with a Chern number $C = 1/2$, which can persist in the presence of weak many-body interactions. These reveal that neutral-atom arrays can emulate fractional Chern insulators. Finally, we also study the proposed two-dimensional hard-core boson model under different theoretical parameter settings; the results further support that the generated nonzero phases associated with hopping amplitudes can produce a stable fractional Chern insulator state theoretically.

DOI: [10.1103/PhysRevA.108.053107](https://doi.org/10.1103/PhysRevA.108.053107)

I. INTRODUCTION

Quantum simulation of condensed-matter physics via atomic, molecular, and optical methods has become an interesting topic recently [1–4]. Among various phases of condensed matter, topological phases [5,6] are especially interesting not only because of their relevance for fundamental condensed matter physics [7–9], but also due to their potential in quantum computing [10,11]. Natural topological phases of matter are not easily manipulated, but it is possible to engineer spin-orbit coupling [12,13] or pseudomagnetic fields [14–22] to prepare topological phases, especially with neutral atoms [23–33].

In this article, we show that it is possible to use van der Waals interaction between Rydberg atoms [34–37] in a two-dimensional array to simulate a topological Chern insulator [38,39] with a fractional Chern number $C = 1/2$. The method depends on an effective magnetic field created by off-resonantly addressing of Rydberg states as proposed in Ref. [40]. A Rydberg state refers to a state where the atomic energy is much higher than its ground-state energy. Because the electron of a Rydberg atom is extended far from its nucleus, the dipole-dipole interaction between two Rydberg atoms is much larger than that between two ground-state atoms [41]. Due to the strong dipole-dipole interaction, there have been intense efforts directed to the search for exotic effective magnetic phases of atoms in dipole microtraps or optical lattices via Rydberg interactions [42–49]. The possibility to realize topological states in a one-dimensional system by Rydberg atoms was demonstrated in [50].

The two-dimensional topological state in our method results from an off-resonant addressing of ground states to Rydberg states [45,46,51–58], so that the effective ground-state atoms inherit interactions from the Rydberg states. Our goal is to design a tight-binding Hamiltonian which has one

or more bands that are topological nontrivial, i.e., possessing nonzero Chern numbers when the time-reversal symmetry is absent. The first step to achieve this is to build up quasiparticle hopping between atoms, and the second is, as one choice, to induce a pseudomagnetic field so that the time-reversal symmetry is broken. In our model, the hopping between two sites is realized by the exchange interaction [41,59–61] when two interacting atoms are in different Rydberg levels, while the pseudomagnetic field can be created via the phase difference of lasers upon the two atoms [40]. Since the atomic spacing in our model is on the order of 10 μm , the benefit of realizing topological band structure via van der Waals interactions is that accurate control of a single atom in the array can be easily carried out [62], thus rendering easier ways to, for instance, study impurities [63] in topological phases and manipulate excitations for topological quantum computation [31,64,65]. Compared to other methods by using direct dipolar exchange interactions of Rydberg atoms [47,48], the Rydberg dressing in this work renders long coherence times for the quasiparticles [45,46,50–57].

The remainder of this article is outlined as follows. In Sec. II we address the technical details of the off-resonant addressing of ground states to Rydberg states and deduce the effective Hamiltonian of the system which describes interacting hard-core bosons on a honeycomb lattice. We also address the possibility of realizing the topological state and specify the parameters. Section III describes the technical details of experimental design with numerical support. Then we generalize the experimental parameter settings to give a purely theoretical study of the proposed effective Hamiltonian. Section IV A briefly addresses the method of producing a flat energy band and gives the parameter settings. In Sec. IV B we prove the existence of a fractional Chern insulator (FCI) phase and propose the parameter settings for the theoretical realization of the FCI phase in this model by using the

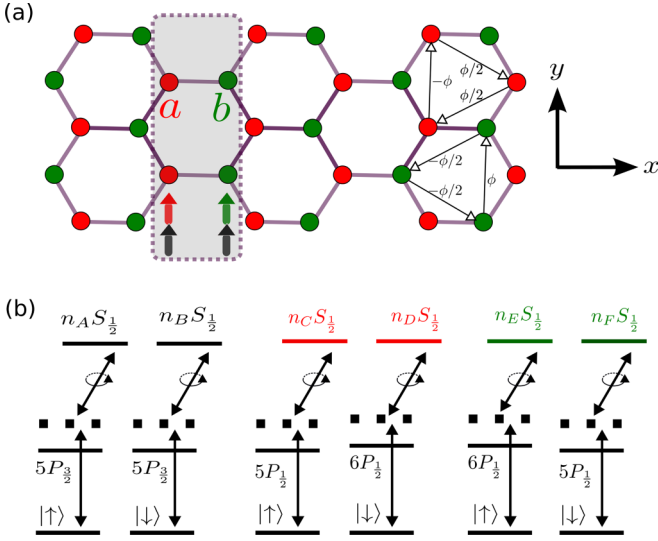


FIG. 1. (a) Quantum emulation of a two-dimensional hard-core boson-Hubbard model in a honeycomb lattice. The numbers $\pm\phi$ and $\pm\phi/2$ show the phase changes when hard-core bosons hop from one site to another, shown by the arrows. (b) Optical admixing of Rydberg states with two ground states for each atom in the dipole microtraps. For each atom, two chosen ground states are excited by two-photon transitions. Each two-photon process is realized by a \mathbf{z} -polarized laser (lower transition) that travels along \mathbf{y} and a right-hand polarized laser (upper transition) that travels along \mathbf{z} . On sublattice a three laser fields are used to address the transition from the ground to the $5P$ states, which in principle can all be the $5P_{3/2}$ state when different detunings at it are used. However, the energy separation between neighboring F states of $5P_{3/2}$ is in the range of 72–267 MHz, and it is useful to tune the two lower lasers for addressing n_A and n_B states to be above the $F = 3$ state and below $F = 0$ states, respectively, or vice versa. Then the $5P_{1/2}$ state is shown for addressing the n_C Rydberg state so as to simplify the tuning of the effective Rabi frequencies and the two-photon detunings for the Rydberg addressing. Similarly, on sublattice b, the $5P_{1/2}$ state is shown for addressing the n_F Rydberg state.

exact diagonalization (ED) and the infinite-size variant of the Density Matrix Renormalization Group (iDMRG) method, and discuss the phase transitions between the FCI phase and other topological trivial phases. Section V gives a brief summary.

II. A HONEYCOMB RYDBERG-DRESSED SYSTEMS WITH EFFECTIVE MAGNETIC FIELDS

We focus on a honeycomb configuration of the dipole microtraps, where the two sublattices are labeled as a and b, as shown in Fig. 1(a). Trapped at each site of the array is one ^{87}Rb atom that is optically excited off-resonantly. Each atom is prepared in a superposition state of two hyperfine ground states $|\uparrow\rangle$ and $|\downarrow\rangle$. These two states can be chosen as $|5S_{1/2}, F = 1(2), m_F = 1\rangle$, where F and m_F denote hyperfine and magnetic quantum numbers, respectively. The nearest-neighboring couplings are realized by coupling the two ground states to two Rydberg levels ($n_A S_{1/2}, n_B S_{1/2}$) for all sites, where $n_B - n_A = 1$. All the coupled Rydberg states have electron and nuclear spin states $1/2$ and $3/2$, respec-

tively, thus these quantum numbers are suppressed in the notations. The van der Waals interaction can drive the two-atom state $|n_A S_{1/2} n_B S_{1/2}\rangle$ to $|n_B S_{1/2} n_A S_{1/2}\rangle$ [41], where the symbols inside the ket on the left and right denote states of the two neighboring atoms. When addressed to the ground states, this type of exchange process results in exchange interaction $|\uparrow\downarrow\rangle \leftrightarrow |\downarrow\uparrow\rangle$ between two neighboring atoms. Since the van der Waals interaction scales as $1/r^6$ at sufficiently large interatomic distances, with r the distance between two atoms, the addressing of the ground states to these two levels will lead to nearest-neighboring effective interaction, while next-nearest neighboring interaction is much smaller. In order to switch on next-nearest neighboring couplings, the ground states are also coupled to two other pairs of Rydberg levels ($n_C S_{1/2}, n_D S_{1/2}$) and ($n_E S_{1/2}, n_F S_{1/2}$) for the two sublattices, respectively, where $n_D - n_C = n_F - n_E = 1$. Since the distance between two next-nearest neighboring sites are $\sqrt{3}$ larger compared to that between two nearest neighbors, n_C, \dots, n_F shall be larger than n_A and n_B , so that the coupling between two nearest sites and that between two next-nearest sites are comparable in magnitude.

The comparable couplings for both nearest and next-nearest neighbors are realized by choosing appropriate Rydberg levels. Even the blockade interaction occurs between two atoms in any Rydberg levels, the exchange interaction occurs only for a pair of levels n_α, n_β when $|n_\alpha - n_\beta|$ is small. As shown in Ref. [66], the van der Waals interaction that exchanges the two principal quantum numbers n_α and n_β is negligible when $|n_\alpha - n_\beta| > 2$. When we choose the condition $n_C - n_B, n_E - n_D > 2$, the exchange process between ($n_A S_{1/2}, n_B S_{1/2}$), ($n_C S_{1/2}, n_D S_{1/2}$), or ($n_E S_{1/2}, n_F S_{1/2}$) is the dominant exchange interaction. This design can give us a large degree of freedom to adjust parameters for simulating different possible magnetic phases [45,46]. Beside of the interaction that exchanges the principal quantum numbers of two atoms, there is a residual interaction that changes the total electron spin of two atoms, but its magnitude is several orders smaller than that of the former process, and thus can be ignored.

The time-reversal symmetry is broken by introducing a nonzero phase to the next-nearest neighboring hopping through the laser excitation. To understand such a phase term for the hopping, we can look at the various optical excitations of the neutral atoms. For all the two-photon transitions depicted in Fig. 1(b), the lower transitions are through linearly polarized lasers, whose electric vectors are polarized along \mathbf{z} , while the upper transitions happen through right-hand polarized laser fields. Now the two-dimensional array lies in the x - y plane, and then it is convenient to choose $z = 0$ for the plane where the atomic array lies. As a result, the phase term with a chosen two-photon Rabi frequency is solely determined by the lower Rabi transition. As an example, consider two general next-nearest sites at \mathbf{r}_1 and \mathbf{r}_2 , respectively; the phase is

$$(\mathbf{k}_{5S_{1/2}, F=1 \rightarrow 5P_{1/2}, F=1} - \mathbf{k}_{5S_{1/2}, F=2 \rightarrow 6P_{1/2}, F=1}) \cdot \mathbf{r}_1 - (\mathbf{k}_{5S_{1/2}, F=1 \rightarrow 5P_{1/2}, F=2} - \mathbf{k}_{5S_{1/2}, F=2 \rightarrow 6P_{1/2}, F=2}) \cdot \mathbf{r}_2, \quad (1)$$

where the wave vectors are along $\hat{\mathbf{y}}$ as indicated by red or green in Fig. 1. For sublattice a, we denote the phase term accompanying the transition from $|\uparrow(\downarrow)\rangle$ to $|n_{C(D)} S_{1/2}\rangle$

as $\phi(\mathbf{r}_i)[\varphi(\mathbf{r}_i)]$ by the two-photon laser excitation as in Fig. 1(b). By performing a perturbation calculation as from Refs. [67,68], the phase term that appeared in $|\uparrow\downarrow\rangle\langle\downarrow\uparrow|_{ij}$ for the effective Hamiltonian reads $\phi_{ij} = \phi(\mathbf{r}_i) - \phi(\mathbf{r}_j) - \varphi(\mathbf{r}_i) + \varphi(\mathbf{r}_j)$. In the setup of Fig. 1(b), the two-photon transitions to $(n_C S_{1/2}, n_D S_{1/2})$ are via $5P_{1/2}$ and $6P_{1/2}$ intermediate levels, giving $\phi_{ij} \sim (E_{5P} - E_{6P})/(\hbar c) \hat{\mathbf{y}} \cdot (\mathbf{r}_i - \mathbf{r}_j)$, with \hbar the reduced Planck constant, c the speed of light in vacuum, and $E_{5(6)P}$ the energy of the atomic level. Because the $5P_{1/2}$ and $6P_{1/2}$ levels have an energy difference of about $2\pi \times 333.9$ THz [69], a significant phase ϕ_{ij} can appear. More details about such phases can be found in Ref. [40] or the Appendix.

The effective Hamiltonian is derived in a perturbative method. When the two-photon detuning is large compared to the two-photon Rabi frequency, the coupling between the ground and the excited states is removed effectively by a canonically transformation [67]. Details of the derivation can be found in Ref. [40]. Up to fourth order, the effective Hamiltonian is given by

$$\hat{H}_{\text{eff}}^{(4)} = \sum_{\alpha, \beta, \gamma, \epsilon = \uparrow, \downarrow} H_{\alpha\beta, \gamma\epsilon} |\alpha\beta\rangle\langle\gamma\epsilon|, \quad (2)$$

where $H_{\alpha\beta, \gamma\epsilon}$ is a function of the Rabi frequency, detuning, and Rydberg interaction [40]. Because the state-changing Rydberg interactions exchange only the states of two interacting atoms and by no means create extra up or down states, one can define hard-core bosons in such types of systems. We note that for a system with dipolar interactions, similar hard-core boson Hubbard models were studied that can be topologically nontrivial [21,22,70,71]. Defining $b_i^\dagger \equiv (|\uparrow\rangle\langle\downarrow|)_i$ and $\hat{n}_i = b_i^\dagger b_i$ for each site i , the system has an effective Hamiltonian $\hat{H}_b = \hat{H}_{\text{tunneling}} + \hat{H}_{\text{blockade}} + \hat{H}_{\text{chemical}}$, where

$$\begin{aligned} \hat{H}_{\text{tunneling}} &= \sum_{\langle i, j \rangle} (t_{ij} b_i^\dagger b_j + \text{H.c.}) \\ \hat{H}_{\text{blockade}} &= \sum_{\langle i, j \rangle} U_{ij} \hat{n}_i \hat{n}_j \\ \hat{H}_{\text{chemical}} &= \sum_i \mu_i \hat{n}_i, \end{aligned} \quad (3)$$

and $\mu_i = \sum_{j \neq i} [(H_{\uparrow\downarrow, \uparrow\downarrow} + H_{\downarrow\uparrow, \downarrow\uparrow})/2 - H_{\downarrow\downarrow, \downarrow\downarrow}]_{i, j}$, $U_{ij} = [H_{\uparrow\uparrow, \uparrow\uparrow} + H_{\downarrow\downarrow, \downarrow\downarrow} - H_{\uparrow\downarrow, \uparrow\downarrow} - H_{\downarrow\uparrow, \downarrow\uparrow}]_{i, j}$, and $t_{ij} = H_{\uparrow\downarrow, \downarrow\uparrow}$. For convenience, we label the nearest-neighboring (N) and next-nearest-neighboring (NN) hoppings arising from the phase-free exchange interactions of Rydberg atoms in states $(n_A S_{1/2}, n_B S_{1/2})$ by t_N and t_{NN} , respectively. The magnitudes of the phase-carrying NN hoppings in sublattices a and b are $t_{NN}^{(aa)}$ and $t_{NN}^{(bb)}$, respectively, while the phase ξ accompanying these hoppings is illustrated in Fig. 1. With these parameters, $t_{ij} = t_N$ for two nearest-neighboring atoms, and $t_{ij} = t_{NN} + t_{NN}^{(xx)} e^{i\xi}$, where $x = a$ or b and ξ is a phase determined by x and the orientation of the two sites. The chemical potential and the NN many-body interaction are $\mu^{(x)}$ and $U_{NN}^{(x)}$ for sublattice x , where $x = a$ or b , while the nearest-neighboring many-body interaction is $U_N^{(ab)}$. These interactions are nonzero in general, indicating that it is

possible to realize interesting many-body phases through van der Waals interactions of neutral atoms.

III. EXPERIMENTAL PROSPECTS

In this section we discuss the experimental prospects for realizing the model of this paper.

First, the excitation of the Rydberg states with $m_J = 1/2$ requires high polarization purity of the laser fields for exciting the atoms. For example, the n_A Rydberg state used in the setup of Fig. 1 can be $|[n_A S_{1/2}] m_J = 1/2, m_l = 3/2\rangle$ in the ideal case. When the lower laser field is not purely \mathbf{z} -polarized, and the upper laser is not purely σ^+ polarized, the Rydberg states $|[n_A S_{1/2}] m'_J, m'_l\rangle$ with $(m'_J, m'_l) = (-1/2, -1/2), (1/2, -3/2), (\pm 1/2, \mp 1/2), (1/2, 1/2), (-1/2, 3/2)$ can be excited. These states can lead to a fourth-order Hamiltonian that has extra terms compared to the desired one, as shown in the Appendix. To achieve the topological model shown above, it is necessary to have high polarization purity. In the supplemental material of Ref. [72] it was shown that with Glan-Taylor polarizers, the intensity polarization purity of a circular light field can be up to $I_+/I_- = 10^4$, which means that the electric field of the wrong polarization is about 1% of that of the correct polarization. If it is used to realize the model of this paper, the undesired Rydberg excitation (corresponding to the excitation by Rabi frequencies with subscripts; see Sec. 2 of the Appendix) will lead to extra terms that are I_-/I_+ times the correct terms and can be significantly suppressed.

The model presented requires the laser fields traveling along the \mathbf{x} - \mathbf{y} plane not to have a significant crosstalk. As shown in Fig. 1(a), the laser pathways addressing sublattices a and b can have a separation $L/2$, which is $6.4 \mu\text{m}$ for the model shown above. To avoid the crosstalk, the Rayleigh range should be large. For example, a Rayleigh range of $X = 26 \mu\text{m}$ was employed in Ref. [73] for single-site addressing in a 3D atom array via lasers of waists $w_0 = 2.7 \mu\text{m}$. By assuming this setup, the ratio between the electric field strength at the nontarget site and that at the beam waist is below $X/\sqrt{X^2 + x^2} \exp\{- (L/2)^2 X^2 / [w_0^2 (X^2 + x^2)]\}$ [40], where x is the axial separation from the beam waist. This ratio is smaller than 0.004 even if $x = 0$ and will drop quickly for larger x . So it is possible to realize the model with the setup of Fig. 1.

The observation of the topological order of the model hinges on the possibility to preserve the coherence of the system. If the dephasing is only from the Rydberg-state decay, then there is no problem as discussed in Ref [40]. However, it is necessary to avoid dephasing due to the dipole-dipole coupling. As shown above, the model depends on pure van der Waals interactions, which is derived by the second-order perturbation theory, shown in the Appendix. In this case it is necessary to set the distance between two atoms far enough so that when they are excited to Rydberg states, their states will not go out of the state manifold covered by the optical excitation. In the Appendix the critical distances for the pairwise interaction to be of the van der Waals type are listed, which indicate that the lattice constant employed in the example can satisfy the condition for the van der Waals interaction. For smaller atomic spacings, dipole-dipole

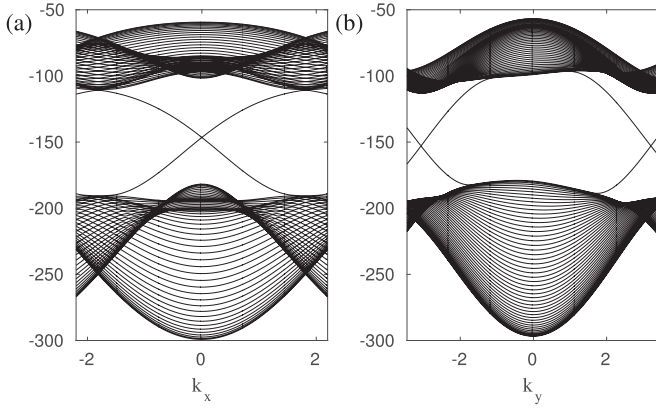


FIG. 2. Energy spectra as a function of wave vector for the Hamiltonian (3) with $U_{ij} = 0$ when the system is on a cylinder, whose axis is along \mathbf{y} and \mathbf{x} in (a) and (b), respectively. The parameters are from the example system in the text. Each finite system here has 50 rows of atoms.

interactions will couple the states to other states that cannot be excited back to the ground state, leading to population loss [74]. However, because the experiments on Rydberg atoms were usually at room temperature, the presence of the thermal photons can couple the excited Rydberg states to nearby Rydberg states that can no longer be coupled back to ground states. This type of dephasing was studied in Ref. [75]. Nonetheless, it is unclear whether this type of blackbody-radiation-induced excitation of Rydberg states will destroy the appearance of the topological order for the model here.

In order to examine the topological property of the system, it is useful to perform a Fourier transform of the single-particle part of Eq. (3), i.e., with $U_{ij} = 0$. Direct calculation gives $H_{\mathbf{k}} = \epsilon(\mathbf{k}) + \sum_{j=1}^3 d_j(\mathbf{k})\sigma^j$, where σ^j is the j th Pauli matrix, and the details can be found in Sec. IV A. To show that it is possible to realize the topological bands with the Hamiltonian in Eq. (3), we choose an example system with the following Rydberg states: $(n_A, n_B, n_C, n_D, n_E, n_F) = (85, 86, 100, 101, 105, 106)$. Using a numerical search with the restriction that the width of the energy band should be flat as proved in Ref. [19], as shown in Fig. 2, we find that a relatively flat Chern band is realized with the lattice constant $L = 12.798 \mu\text{m}$, $(\Omega_A, \Omega_B, \Omega_C, \Omega_D, \Omega_E, \Omega_F)/2\pi = (-102.8, 397.2, 1947.4, 386.1, 975.4, 1357.8)$ kHz, $\Delta_\alpha/\Omega_\alpha = \eta$, with $\eta = 7.90, 7.27$, and 8.34 when $\alpha = (A, B), (C, D)$, and (E, F) , respectively; see the Appendix for details. With these parameters, the upper band is narrow: the gap between these two bands is 1.52 times of the width of the upper band. The parameters of the hard-core boson model of Eq. (3) are $\phi = 49.377\pi$ rad, $(\mu^{(a)}, \mu^{(b)}, t_{\text{NN}}, t_{\text{NN}}^{(aa)}, t_{\text{NN}}^{(bb)}, t_{\text{N}})/2\pi = (-159, -152, 2, 12, 12, -40)$ Hz, and $(U_{\text{NN}}^{(aa)}, U_{\text{NN}}^{(bb)}, U_{\text{N}}^{(ab)})/2\pi = (-9.15, -9.96, 92.7)$ Hz. These couplings are much larger than the decoherence rate of the state $|\uparrow(\downarrow)\rangle$ [40]. The upper band has a width of $2\pi \times 47.0$ Hz, while the gap between the lower and upper bands is $2\pi \times 71.4$ Hz. Indeed, dispersionless edge states can appear at the boundary of a topological band insulator. This is confirmed when we put the system on a cylinder. As shown in Fig. 2(a) with an

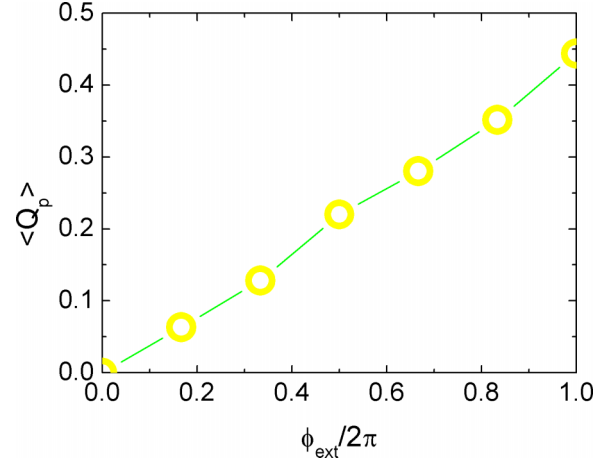


FIG. 3. Charge pumping with respect to the external flux ϕ_{ext} under the proposed experimental parameter setting.

armchair boundary and in Fig. 2(b) with a zigzag boundary, there are two curves connecting the lower and upper bands. It is straightforward to check that the Chern number of the two bands is ± 1 ; however, for the experimental case, the generating of mutual couplings between atoms are inevitable. Therefore, we have to turn to a numerical simulation of the interacting cases by taking all the U couplings into consideration.

To check the validity of realizing a topological insulator concerning the above experimental parameter setting, we calculated the charge pumping $\langle Q_p \rangle$ with respect to the external flux ϕ_{ext} by implementing the iDMRG method; see Sec. IV B for technical details. A finite value of $\langle Q_p \rangle$ denotes the nontrivial topological effect of the model and gives the topological charge simultaneously. As shown in Fig. 3, the model with our proposed parameters for experimental design reproduces the charge pumping phenomena successfully; we can see that $\langle Q_p \rangle \sim 0.5$ considering the numerical instability. Figure 3 indicates that our proposed parameter setting may lead to a fractional Chern insulator state; in consequence, we give a thorough theoretical study of Eq. (3) by generalizing the experimental parameter settings in the following sections and further confirm the existence of a stable fractional Chern insulator phase in such a model.

IV. THEORETICAL GENERALIZATION

Although we have proved that a fractional Chern insulator can be realized by using Rydberg-dressed neutral atoms, which is described effectively by Eq. (3), the alternation of parameters is confined to experimental settings. Therefore, it is still necessary to set the theoretical foundation that a model with respect to Eq. (3) can really generate a stable fractional quantum Hall state, which is exactly the aim of this section.

A. Topologically flat bands

Equation (3) is analogous to the Haldane-Bose-Hubbard model [6, 19] filled with hard-core bosons except for the different phase factors pertaining to the next-nearest hopping $t_{\text{NN}}^{(aa)}$ and $t_{\text{NN}}^{(bb)}$ that generate zero net flux threading within one unit

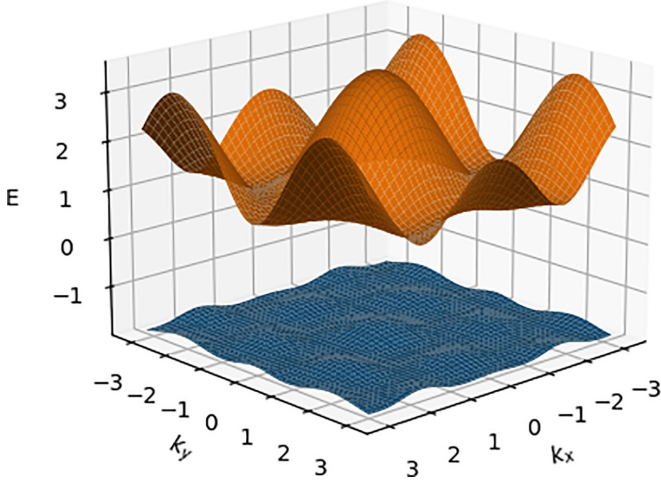


FIG. 4. Band structure of Eq. (3) for which the flatness ratio for the ground energy band is 0.099, and $t_N = -1$, $\phi = 8.37700016$, $t_{NN}^{(aa)or(bb)} = -0.31$, $t_{NN} = 0.14$.

cell, as shown in Fig. 1(a). We will name our model described by Eq. (3) as the untypical Haldane-Bose-Hubbard (UHB) model in the following context for convenience in comparison with the usual Haldane-Bose-Hubbard model. Previous studies [19,76] of the Haldane-Bose-Hubbard model have shown that a fractional Chern insulator (FCI) phase with a fractional Chern number $C = 1/2$ can be realized in such a model with parameter settings under which a flat ground energy band is achieved. Such a model is termed as topological flat band model (TFB). Consequently, it is natural to expect that such a FCI phase may also be realized in the UHB model.

Since the existence of flat bands is the prerequisite for the FCI phase to appear, it is useful to show a set of parameters for Eq. (3) to support TFB. The flat ground energy band is described by the flatness ratio, which is defined as δ/Δ [20], where δ is the band width of the ground energy band and Δ denotes the energy gap above the ground energy band. In the noninteracting case, Eq. (3) can be directly diagonalized by means of Fourier transformation, which gives $H_{\mathbf{k}} = d_0(\mathbf{k}) + \sum_{j=1}^3 d_j(\mathbf{k})\sigma^j$, where σ^j is the j th Pauli matrix, and

$$\begin{aligned} d_0 &= 2t_2 \left(\cos \phi \cos \mathbf{k}\mathbf{v}_1 + \cos \frac{\phi}{2} \cos \mathbf{k}\mathbf{v}_2 + \cos \frac{\phi}{2} \cos \mathbf{k}\mathbf{v}_3 \right), \\ d_1 &= t(\cos \mathbf{k}\mathbf{s}_1 + \cos \mathbf{k}\mathbf{s}_2 + \cos \mathbf{k}\mathbf{s}_3), \\ d_2 &= t(\sin \mathbf{k}\mathbf{s}_1 + \sin \mathbf{k}\mathbf{s}_2 + \sin \mathbf{k}\mathbf{s}_3), \\ d_3 &= 2t_2 \left(-\sin \phi \sin \mathbf{k}\mathbf{v}_1 + \sin \frac{\phi}{2} \sin \mathbf{k}\mathbf{v}_2 + \sin \frac{\phi}{2} \sin \mathbf{k}\mathbf{v}_3 \right). \end{aligned}$$

Here $\mathbf{v}_1 = (\sqrt{3}, 0)$, $\mathbf{v}_{2,3} = (-\sqrt{3}/2, \pm 3/2)$, and $\mathbf{s}_{1,2} = (\pm\sqrt{3}/2, 1/2)$, $\mathbf{s}_3 = (0, -1)$. Then the two eigenvalues of $H_{\mathbf{k}}$ can be written as $\varepsilon_{\pm, \mathbf{k}} = d_0(\mathbf{k}) \pm \sqrt{d_1^2(\mathbf{k}) + d_2^2(\mathbf{k}) + d_3^2(\mathbf{k})}$. We can read out the band width of the lower band $\varepsilon_{-, \mathbf{k}}$, $\delta = \max[\varepsilon_{-, \mathbf{k}}] - \min[\varepsilon_{-, \mathbf{k}}]$, and the energy gap, $\Delta = \min[\varepsilon_{+, \mathbf{k}}] - \max[\varepsilon_{-, \mathbf{k}}]$. The band flatness ratio δ/Δ can be obtained numerically, and the optimal value for it is fixed at about 0.099 with the parameter setting $t_N = -1$, $\phi = 8.37700016$, $t_{NN}^{(aa)} = t_{NN}^{(bb)} = -0.31$, $t_{NN} = 0.14$, as shown in Fig. 4. Here, by fol-

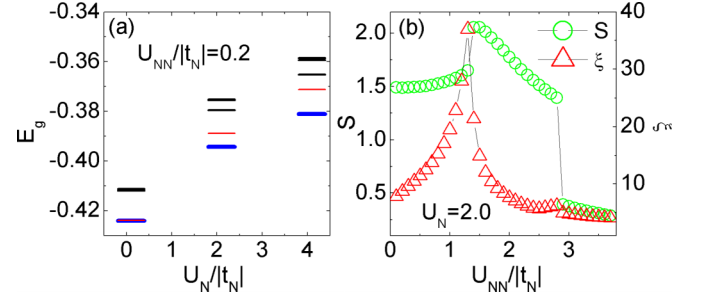


FIG. 5. (a) ED results of the lowest six eigenlevels of a half-filling 4×3 lattice for $U_N = 0.1, 2.1, 4.1$ with $U_{NN} = 0.2$, of which the blue lines denote the ground energy level and the red lines indicate the first excitation energy. (b) Von Neumann entropy and the correlation length of the system with respect to U_{NN} with $U_N = 2.0$. The data were obtained with iDMRG calculations on an infinite cylinder with MPS unit cell of size 4×4 and the bond dimension χ up to 200.

lowing Ref. [19], we have taken the next-nearest-neighbor hopping terms t_{NN} between different sublattices into consideration in order to obtain a more flatter band structure.

Next, in the following section, we will search for the expected FCI phase and its robustness to the finite coupling $U_N^{(ab)}$ and $U_{NN}^{(a)or(b)}$, which will be abbreviated as U_N and U_{NN} , respectively, in the above TFB UHB model and briefly discuss the nontopological phases exhibited in its phase diagram.

B. Numerical results

In this section we perform the ED and iDMRG calculations to ascertain the possible phases exhibited by the UHB model with a flat ground energy band and demonstrate the existence of a FCI phase in the phase diagram of the model with respect to U_{NN} and U_N ; here we will set $|t_N| = 1$ as the energy scale. The stability of this FCI phase against the presence of finite interactions and the phase transitions driven by the ratio of U_{NN}/U_N are also studied numerically.

To facilitate the numerical calculation and utilize the translational symmetry of the UHB model, we roll the honeycomb array shown in Fig. 1(a) as an infinite cylinder along the x axis while with a finite circumference L_y unit cells along the y direction. For the ED calculation, we will consider a 3×4 ($L_y \times L_x$) lattice with a periodical boundary along both of the space directions.

We concentrate on the half-filling Hilbert subspace with the filling factor $\nu = N_b/N_{\text{cell}} = 1/2$, where N_b is the particle number and N_{cell} is the total number of unit cells of the lattice. It has been verified for the TFB Haldane-Bose-Hubbard model that the ground state with $\nu = 1/2$ in the weak coupling case is a $1/2$ bosonic fractional Chern insulator [19]. Therefore, a $1/2$ bosonic FCI state is also naturally expected in our model due to its analogy to the usual Haldane-Bose-Hubbard model.

First, we determine the phase diagram of the TFB UHB model with respect to different U_N and U_{NN} . Figure 5(a) displays the selected sets of energy spectrum of the TFB UHB model obtained by ED calculations. For conciseness, we put only the first lowest six eigenvalues for each pair of

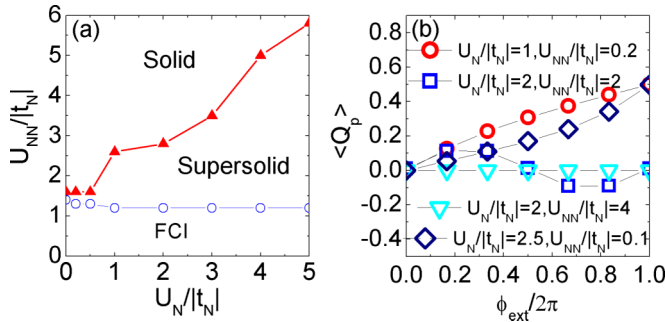


FIG. 6. (a) Phase diagram of model 3. (b) Charge excitation with respect to the external flux ϕ_{ext} under distinct parameter settings. We amplified the curve corresponding to the scale of $U_N = 2$ and $U_{NN} = 2$ by 1000 times to show its behavior clearly. All the data were obtained by iDMRG calculations with an infinite cylinder with MPS bond dimension χ up to 600.

(U_{NN} , U_N) in the figure. We find that, when $U_{NN} \leq 1$, the ground energy is nearly double degenerated, and this double manifold is separated by a moderate finite gap to the lowest exciting energy level. This kind of double degeneracy is a necessary condition for the occurrence of a FCI state and is consistent with the ED results of Ref. [19]. However, such a double degeneracy will be slightly lifted by increasing either U_N , which inevitably introduces numerical instability to the determination of the FCI phase.

Figure 5(b) presents the critical behaviors of the von Neumann entanglement entropy and the correlation length for the TFB HUB model obtained by iDMRG calculations. With a fixed $U_N = 2.0$, the system driven by the next-nearest neighbor coupling U_{NN} exhibits two critical points: the first one at $U_{NN} = 1.3$ is signified by a sharp peak of the correlation length and a clear jump of the von Neumann entanglement entropy which implies a second-order quantum phase transition; by contrast, the correlation length near the other critical point at $U_{NN} = 2.8$ shows only a jump behavior together with the von Neumann entanglement entropy implying a first-order phase transition.

Figure 6(a) plots the phase diagram of the UHB model with respect to U_N and U_{NN} , which is obtained by combining the data from Figs. 5(a) and 5(b). There are three distinct phases: one FCI phase at the bottom of the phase diagram, one supersolid phase, and a solid phase. The topological nature of the FCI phase is of particular interest as shown below.

To determine the topological properties of the FCI region in Fig. 6(a), we resort to the infinite density matrix renormalization group (iDMRG) method to study the charge excitation effect as in Laughlin's gedanken experiment [77]. Technically, we add the external magnetic flux ϕ_{ext} threading through the cylinder, which can be realized by imposing twist boundary conditions along the y direction in the model during iDMRG calculation. Then we adiabatically evolve the ϕ_{ext} from 0 to 2π , which means one has to calculate the ground-state wave function with respect to each value of the ϕ_{ext} in sequence by utilizing the wave function obtained in the last DMRG step as the initial trial wave function. After the adiabatic evolution and due to the particle hopping between the edge modes [78] in the topological FCI phase, the ground state is restored to

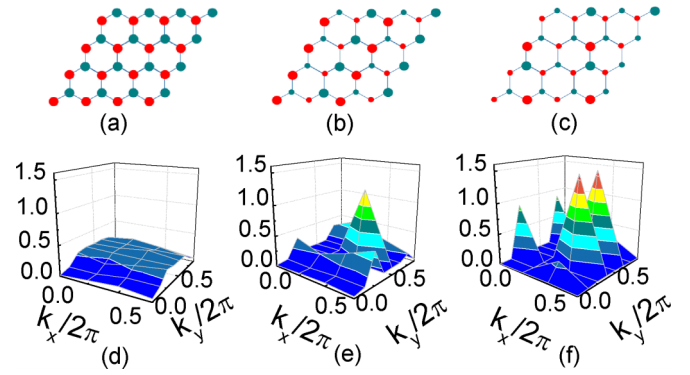


FIG. 7. The corresponding on-site charge distribution in the phase diagram. Red and blue dots denote different sublattices, and the magnitude of the on-site charge density is signified by the diameter of the dots. (a) FCI phase and the topological trivial phase with $C = 0$ with $U_N = 2$ and $U_{NN} = 0.2$ (b) Supersolid phase with $U_N = 2$ and $U_{NN} = 2$. (c) Solid phase with $U_N = 2$ and $U_{NN} = 4$. The data were obtained from iDMRG calculations. Panels (d), (e), and (f) plot the corresponding structure factors to (a), (b), and (c).

the one before the insertion of ϕ_{ext} but with a different particle distribution which leads to the passing of $\langle Q_p \rangle$ particles across the middle cut point of the matrix product state (MPS) wave function on the cylinder; here $\langle Q_p \rangle$ featuring the quantized Hall conductivity just gives the Chern number of the topological phase, and we find that it is exactly $1/2$ as illustrated in Fig. 6(b) for the case of $U_N = 1$, $U_{NN} = 0.2$. This demonstrates the existence of a FCI phase in the TFB UHB model.

The stability of the FCI state with respect to internal or external factors has been investigated in many previous works, e.g., Ref. [79]; in the article we also ascertain that the charge pumping effect associated to the FCI phase is also not stable in the presence of the nearest-neighboring coupling U_N . Figure 5(a) reveals that the double ground state degeneracy can be lifted by a larger $U_N > 1$; further calculation confirms that U_{NN} can also lift the degenerated ground energy manifold. Therefore, in order to obtain the charge pumping phenomena, we have to increase both the truncate dimension and the size of the unit cell along the y direction during the iDMRG calculation. In Fig. 6(b), as an example, we plot the result for the case of $U_{NN} = 0.1$ with $U_N = 2.5$. However, this numerical instability cannot be detected by using the criteria of correlation length or von Neumann entanglement entropy; the ground-state on-site particle occupancy pattern in the FCI phase shows uniform charge distribution with an on-site charge density of $\langle n_i \rangle = 1/4$ as shown in Fig. 7(a).

By increasing U_{NN} , we also find two topological trivial phases: the supersolid phase and the solid phase as illustrated in Fig. 6(a), which is very analogous to the scenario in Ref. [76]. The on-site particle density and the corresponding structure factor $S(\mathbf{q})$ for these two phases are shown in Figs. 7(b) and 7(c). The supersolid phase is characterized by the (π, π) peak of $S(\mathbf{q})$ and the sinusoidal pattern of charge excitation as shown in Fig. 6(b). The supersolid phase is driven into the solid phase by increasing U_{NN} across a first-order phase transition as indicated in Fig. 5(b). In such a solid phase, the charge excitation effect disappears as

shown in Fig. 6(b), and a large gap shows up in the entanglement spectrum above the lowest energy of which the data are not shown here. A difference with Ref. [76] is that the two peaks of $S(\mathbf{q})$ at $(\pi, \pi/2)$ and $(\pi, 3\pi/2)$ are shifted to $(\pi, \pi/4)$ and $(\pi, 3\pi/4)$, which is due to the physical effect of the special complex hopping phase factors of the UHB model. The conclusions about these two phases are almost the same as the results of Ref. [76], and no further discussion is necessary here.

V. CONCLUSIONS

In summary, we propose a method to simulate a fractional Chern insulator based on Rydberg-dressed neutral atoms. By using Rydberg dressing, a hard-core boson Hubbard model with a special complex hopping amplitudes on a honeycomb array can be realized. With the help of massive numerical searching, we find a set of parameters which may be experimentally suitable to be implemented to simulate a fractional Chern insulator whose ground energy band can be described by a fractional Chern number of $1/2$ concerning their topology, and the conclusion is justified by numerical calculations. Nevertheless, it should be noted that the experimental parameter setting cannot be chosen arbitrarily; more effort is needed to put into the work of optimizing the experimental setting in the future. Despite the imposing of the experimental restriction, we give a thorough numerical study of the fractional Chern insulating phase of the model by generalizing the experimental parameter settings. Our results clearly support the existence of a stable FCI phase in the special hard-core boson Hubbard model, dubbed the UHB model in the context, under finite intersite couplings and set a theoretical foundation for the appearance of topological phenomena in a model with the different type of time-reversal symmetry-breaking items that are presented in this article. This shows that anomalous fractional quantum Hall phases may be emulated with neutral atoms via Rydberg dressing.

ACKNOWLEDGMENTS

We thank Shou-Shu Gong and Wei-Wei Luo for very useful discussions. Y.Z. acknowledges support from the Natural Science Basic Research Plan in Shaanxi Province of China under Grant No. 2021JM-041 and Hebei Normal University under Grant No. L2023B06, and X.-F.S. is supported by the National Natural Science Foundation of China under Grants No. 12074300 and No. 11805146, and the Innovation Program for Quantum Science and Technology under Grant No. 2021ZD0302100, and the Fundamental Research Funds for the Central Universities. The iDMRG calculations were performed using the TeNPy Library [80].

APPENDIX: EFFECTIVE HAMILTONIAN VIA RYDBERG DRESSING

1. Rydberg interaction when $n_A \neq n_B$

The proposal hinges on the possibility to create van der Waals interaction between Rydberg atoms. The van der Waals interaction is from the second-order perturbation of dipole-dipole interaction when two atoms A and B are far enough

[41]. For an atomic state highly excited, we use the principal quantum number n , electron angular momentum quantum number l , total angular momentum quantum number j , and magnetic quantum number m to represent its state. Here the quantization axis is along z . The dipole-dipole interaction between two atoms with quantum numbers (n_A, l_A, j_A, m_A) and (n_B, l_B, j_B, m_B) is an electrostatic interactions given by

$$\hat{V}_{dd} = \hat{\mathbf{s}}_A \cdot (3\hat{\mathbf{r}}\hat{\mathbf{r}}/r^2 - \hat{\mathbf{I}}) \cdot \hat{\mathbf{s}}_B/L^3, \quad (\text{A1})$$

where $\hat{\mathbf{s}}_{A(B)}$ is the dipole moment of atom A(B), L the distance between the two atoms, and $\hat{\mathbf{I}}$ an identity operator. Using the representation of spherical harmonic rank 2 tensor, the matrix element

$$V_{m_A m_B; m_a m_b} = \langle n_A l_A j_A m_A; n_B l_B j_B m_B | \hat{V}_{dd} | n_a l_a j_a m_a; n_b l_b j_b m_b \rangle \quad (\text{A2})$$

can be written as

$$- \frac{\sqrt{6}}{L^3} \langle n_A l_A j_A || D_A^{[1]} || n_a l_a j_a \rangle \langle n_B l_B j_B || D_B^{[1]} || n_b l_b j_b \rangle \\ \times \sum_{M=-2}^2 \Psi_{-M}^{[2]}(\theta, \psi) \sum_{\alpha, \beta=-1}^1 C_{\alpha\beta M}^{112} C_{m_a \alpha m_A}^{j_a 1 j_A} C_{m_b \beta m_B}^{j_b 1 j_B}, \quad (\text{A3})$$

where $D_k^{[1]}$ is the dipole moment of atom $k = A$ or B in terms of rank 1 tensor, C a Clebsch-Gordan coefficient, $\Psi^{[2]}$ a rank 2 tensor given by the standard spherical harmonics multiplied by a factor of $\sqrt{4\pi/5}$, and (θ, ψ) the angular position of atom B with respect to atom A. Because all the second-order spherical harmonics, except Ψ_0 , are $\propto \sin \theta$, the dipole coupling will conserve the total projection of the magnetic angular momenta of the two atoms when $\theta = 0$. Here the dipole matrix element $\langle n_A l_A j_A || D_A^{[1]} || n_a l_a j_a \rangle$ can be calculated using the Wigner-Eckart theorem. More details can be found in Ref. [41].

When the coupling strength of the two dipoles is much smaller than the energy difference of the dipole-coupled initial and final two-atom states, the two-atom state is hardly excited out of the degenerate manifold $(n_A, l_A, j_A; n_B, l_B, j_B)$, $(n_B, l_B, j_B; n_A, l_A, j_A)$ for two atoms in different initial fine structures. Even when the principal quantum numbers of the two atoms are not exchanged, their magnetic angular momenta m_A and m_B can still change. In this case, the van der Waals interaction is given by

$$\hat{H}_{vdW} = - \sum_{n_a l_a j_a} \sum_{n_b l_b j_b} \hat{V}_{dd} \hat{V}_{dd}^\dagger / \delta_{ab}. \quad (\text{A4})$$

Here the matrix elements of \hat{V}_{dd} are given in Eq. (A2), and the energy defect is [35]

$$\delta_{ab} = E(n_a l_a j_a) + E(n_b l_b j_b) - [E(n_A l_A j_A) + E(n_B l_B j_B)], \quad (\text{A5})$$

where $E(nl j)$ is the atomic energy of a Rydberg atom with quantum numbers n, l, j . An interesting example is that state $(n_A, l_A, j_A, m_A; n_B, l_B, j_B, m_B)$ can go to state $(n_B, l_B, j_B, m_B; n_A, l_A, j_A, m_A)$, i.e., the quantum numbers of the two atoms swap. In this paper we are interested in such processes when $(l_A, j_A) = (l_B, j_B) = (0, 1/2)$, and the polar angle $\theta = \pi/2$.

Consider two ^{87}Rb Rydberg atoms lying perpendicular to the quantization axis, one prepared in state $|r_{A\pm}\rangle = |n_A\ ^2S_{\frac{1}{2}}, m_J = \pm 1/2\rangle \otimes |m_I\rangle$, and the other in state $|r_{B\pm}\rangle = |n_B\ ^2S_{\frac{1}{2}}, m_J = \pm 1/2\rangle \otimes |m_I\rangle$, where $n_A \neq n_B$. We consider the following four channels for the dipole-dipole interaction, each characterized by its energy defect:

$$\begin{aligned}\delta_1(n_a, n_b) &= E(n_a p_{\frac{3}{2}}) + E(n_b p_{\frac{3}{2}}) - E(n_A s_{\frac{1}{2}}) - E(n_B s_{\frac{1}{2}}), \\ \delta_2(n_a, n_b) &= E(n_a p_{\frac{3}{2}}) + E(n_b p_{\frac{1}{2}}) - E(n_A s_{\frac{1}{2}}) - E(n_B s_{\frac{1}{2}}), \\ \delta_3(n_a, n_b) &= E(n_a p_{\frac{1}{2}}) + E(n_b p_{\frac{3}{2}}) - E(n_A s_{\frac{1}{2}}) - E(n_B s_{\frac{1}{2}}), \\ \delta_4(n_a, n_b) &= E(n_a p_{\frac{1}{2}}) + E(n_b p_{\frac{1}{2}}) - E(n_A s_{\frac{1}{2}}) - E(n_B s_{\frac{1}{2}}).\end{aligned}\quad (\text{A6})$$

Here (n_a, n_b) denote the principal quantum numbers of the pair state produced by the scattering process. These four couplings are known to be the dominant ones in our case. In the van der Waals interaction the atoms then go back to the initial levels and the magnetic quantum number of either atom can change up to 1. We can separate the angular dependence of the interaction from the principal quantum numbers; then Eq. (A4) can be written as

$$\hat{H}_{\text{vdW}}^{(n_A, n_B)} = \sum_{k=1}^4 \sum_{n_a l_a} \sum_{n_b l_b} D(\delta_k) C_6^{(k)}. \quad (\text{A7})$$

When the polar angle $\psi = 0$, the matrix representation of the matrix D in the basis of $|r_{A+}r_{B+}\rangle, |r_{A-}r_{B+}\rangle, |r_{A+}r_{B-}\rangle, |r_{A-}r_{B-}\rangle$ is given by

$$\begin{aligned}D(\delta_1) &= \begin{pmatrix} 0.3457 & 0 & 0 & -0.0741 \\ 0 & 0.2469 & 0.0247 & 0 \\ 0 & 0.0247 & 0.2469 & 0 \\ -0.0741 & 0 & 0 & 0.3457 \end{pmatrix}, \\ D(\delta_{2(3)}) &= \begin{pmatrix} 0.0988 & 0 & 0 & 0.0741 \\ 0 & 0.1975 & -0.0247 & 0 \\ 0 & -0.0247 & 0.1975 & 0 \\ 0.0741 & 0 & 0 & 0.0988 \end{pmatrix}, \\ D(\delta_4) &= \begin{pmatrix} 0.1235 & 0 & 0 & -0.0741 \\ 0 & 0.0247 & 0.0247 & 0 \\ 0 & 0.0247 & 0.0247 & 0 \\ -0.0741 & 0 & 0 & 0.1235 \end{pmatrix},\end{aligned}\quad (\text{A8})$$

where one finds interactions that change the overall magnetic quantum number of the two atoms up to 2 for each scattering process. When the polar angle $\psi = \pi/2$,

$$\begin{aligned}D(\delta_1) &= \begin{pmatrix} 0.3457 & 0 & 0 & 0.0741 \\ 0 & 0.2469 & 0.0247 & 0 \\ 0 & 0.0247 & 0.2469 & 0 \\ 0.0741 & 0 & 0 & 0.3457 \end{pmatrix}, \\ D(\delta_{2(3)}) &= \begin{pmatrix} 0.0988 & 0 & 0 & -0.0741 \\ 0 & 0.1975 & -0.0247 & 0 \\ 0 & -0.0247 & 0.1975 & 0 \\ -0.0741 & 0 & 0 & 0.0988 \end{pmatrix},\end{aligned}$$

TABLE I. Critical distance for the interaction between two atoms at level $n_1 S_{1/2}$ and $n_2 S_{1/2}$ to change from dipole-dipole to van der Waals feature.

$n_1 \setminus n_2$	85	86	100	101	105	106
85	4.0					
86	5.6	4.1				
100	1.5	3.8	6.1			
101	1.2	1.6	7.9	6.2		
105	0.7	0.8	5.7	9.2	6.8	
106	0.6	0.6	5.0	5.9	8.8	7.0

$$D(\delta_4) = \begin{pmatrix} 0.1235 & 0 & 0 & 0.0741 \\ 0 & 0.0247 & 0.0247 & 0 \\ 0 & 0.0247 & 0.0247 & 0 \\ 0.0741 & 0 & 0 & 0.1235 \end{pmatrix}. \quad (\text{A9})$$

We take $(n_A, n_B) = (85, 86)$ as an example, and numerically calculate [66],

$$\hat{H}_{\text{vdW}}^{(85,86)} = \begin{pmatrix} \mathcal{V} & \mathbb{V} \\ \mathbb{V} & \mathcal{V} \end{pmatrix}, \quad (\text{A10})$$

where

$$\begin{aligned}\mathcal{V} &= \begin{pmatrix} 13\,254 & 0 & 0 & \mathcal{V}_f \\ 0 & 12\,447 & 202 & 0 \\ 0 & 202 & 12\,447 & 0 \\ \mathcal{V}_f^* & 0 & 0 & 13\,254 \end{pmatrix} \frac{\mu\text{m}^6 \text{GHz}}{L^6}, \\ \mathbb{V} &= \begin{pmatrix} 10\,350 & 0 & 0 & \mathbb{V}_f \\ 0 & 9\,579 & 193 & 0 \\ 0 & 193 & 9\,579 & 0 \\ \mathbb{V}_f^* & 0 & 0 & 10\,350 \end{pmatrix} \frac{\mu\text{m}^6 \text{GHz}}{L^6},\end{aligned}\quad (\text{A11})$$

where $(\mathcal{V}_f, \mathbb{V}_f) = (303 - 525i, 289 - 501i), (-606, -578), (303 + 525i, 289 + 501i)$ when $\psi = (-\pi/3, 0, \pi/3)$. The basis vectors of $\hat{H}_{\text{vdW}}^{(85,86)}$ for the columns from left to right and for the rows from top to bottom are

$$\begin{aligned}&|r_{A+}r_{B+}\rangle, |r_{A-}r_{B+}\rangle, |r_{A+}r_{B-}\rangle, |r_{A-}r_{B-}\rangle, |r_{B+}r_{A+}\rangle, \\ &|r_{B-}r_{A+}\rangle, |r_{B+}r_{A-}\rangle, |r_{B-}r_{A-}\rangle.\end{aligned}\quad (\text{A12})$$

The critical distance for the interaction between the two atoms to follow Eq. (A11) is $5.6 \mu\text{m}$, which applies to both \mathcal{V} and \mathbb{V} since the perturbation channels for calculating them are the same [66]. The other relevant critical distances are listed in Table I.

When $(n_A, n_B) = (85, 85)$ and $(n_B, n_B) = (86, 86)$, we have

$$\begin{aligned}\hat{H}_{\text{vdW}}^{(85,85)} &= \begin{pmatrix} 8637 & 0 & 0 & v_{85} \\ 0 & 8415 & 55 & 0 \\ 0 & 55 & 8415 & 0 \\ v_{85}^* & 0 & 0 & 8637 \end{pmatrix} \frac{\mu\text{m}^6 \text{GHz}}{L^6}, \\ \hat{H}_{\text{vdW}}^{(86,86)} &= \begin{pmatrix} 9903 & 0 & 0 & v_{86} \\ 0 & 9647 & 64 & 0 \\ 0 & 64 & 9647 & 0 \\ v_{86}^* & 0 & 0 & 9903 \end{pmatrix} \frac{\mu\text{m}^6 \text{GHz}}{L^6},\end{aligned}\quad (\text{A13})$$

where $v_{85} = 83 - 144i, -166, 83 + 144i$ when $\psi = (-\pi/3, 0, \pi/3)$ $v_{86} = 96 - 166i, -192, 96 + 166i$ when $\psi = (-\pi/3, 0, \pi/3)$. Here the basis vectors are

$$|r_{A+}r_{A+}\rangle, |r_{A-}r_{A+}\rangle, |r_{A+}r_{A-}\rangle, |r_{A-}r_{A-}\rangle, \quad (\text{A14})$$

for $\hat{H}_{\text{vdW}}^{(85,85)}$ and

$$|r_{B+}r_{B+}\rangle, |r_{B-}r_{B+}\rangle, |r_{B+}r_{B-}\rangle, |r_{B-}r_{B-}\rangle, \quad (\text{A15})$$

for $\hat{H}_{\text{vdW}}^{(86,86)}$. The critical distance for $\hat{H}_{\text{vdW}}^{(85,85)}$ and $\hat{H}_{\text{vdW}}^{(86,86)}$ is $4.0 \mu\text{m}$ and $4.1 \mu\text{m}$, respectively. When we excite all atoms to both levels $n_A = 85$ and $n_B = 86$, one shall set the distance between any two atoms far compared to these critical distances as in this paper. The relevant data for the states used in this paper are shown in Table I, which show that for the parameters used in the main text, the interactions are of the van der Waals character.

2. Perturbative calculation of the effective Hamiltonian

Consider two atoms labeled as atom 1 and atom 2, where each is prepared in a superposition of the two states $|\uparrow\rangle$ and $|\downarrow\rangle$. Now the state $|\uparrow\rangle$ is excited to states $|r_{A+}\rangle$, while $|\downarrow\rangle$ is excited to states $|r_{B+}\rangle$. In order to show the impact of wrong polarization of the laser fields on the model, we will derive an effective Hamiltonian by assuming that the state $|\uparrow\rangle$ is excited to states $|r_{A\pm}\rangle$, while $|\downarrow\rangle$ is excited to states $|r_{B\pm}\rangle$.

The optical excitation is the perturbation

$$\hat{V} = \frac{1}{2} \sum_k \sum_{\alpha=\pm} (\Omega_{A\alpha} e^{i\phi_{k\alpha}} |\uparrow\rangle \langle r_{A\alpha}| + \Omega_{B\alpha} e^{i\phi_{k\alpha}} |\downarrow\rangle \langle r_{B\alpha}| + \text{H.c.})_k, \quad (\text{A16})$$

where k denotes the index for the atom. After completion of the derivation, we will set Ω_{A-} and Ω_{B-} as zero for demonstrating the physics through a simple excitation scheme. Note that the phase term $\phi_{k\alpha}$ differs from atom to atom. First, it is useful to diagonalize the operator \hat{H}_0 in the two-atom basis. With the $n = 85, 86$ states as an example, the unperturbed Hamiltonian

$$\hat{H}_0 = \sum_i \sum_{\alpha=\pm} [-\Delta_A |r_{A\alpha}\rangle \langle r_{A\alpha}| - \Delta_B |r_{B\alpha}\rangle \langle r_{B\alpha}|]_i + \sum_{(ij)} [\hat{H}_{\text{vdW}}^{(85,85)} + \hat{H}_{\text{vdW}}^{(85,86)} + \hat{H}_{\text{vdW}}^{(86,86)}]_{ij}, \quad (\text{A17})$$

for the two atoms at sites i and j can be diagonalized. There are two different cases.

(a) For the addressing of different Rydberg levels, diagonalization gives the following eigenvalues and eigenstates,

$$E_{1\pm} = -\Delta_A - \Delta_B + \mathcal{V}_b + \mathbb{V}_b \pm (\mathcal{V}_f + \mathbb{V}_f),$$

$$E_{2\pm} = -\Delta_A - \Delta_B + \mathcal{V}_b - \mathbb{V}_b \pm (\mathcal{V}_f - \mathbb{V}_f),$$

$$E_{3\pm} = -\Delta_A - \Delta_B + \mathcal{V}_d + \mathbb{V}_d \pm (\mathcal{V}_e + \mathbb{V}_e),$$

$$E_{4\pm} = -\Delta_A - \Delta_B + \mathcal{V}_d - \mathbb{V}_d \pm (\mathcal{V}_e - \mathbb{V}_e), \quad (\text{A18})$$

and the corresponding eigenstates,

$$\begin{aligned} 2|v_{1\pm}\rangle &= |r_{B-}r_{A-}\rangle + |r_{A-}r_{B-}\rangle \pm (|r_{B+}r_{A+}\rangle + |r_{A+}r_{B+}\rangle), \\ 2|v_{2\pm}\rangle &= |r_{B-}r_{A-}\rangle - |r_{A-}r_{B-}\rangle \pm (|r_{B+}r_{A+}\rangle - |r_{A+}r_{B+}\rangle), \\ 2|v_{3\pm}\rangle &= |r_{B+}r_{A-}\rangle + |r_{A+}r_{B-}\rangle \pm (|r_{B-}r_{A+}\rangle + |r_{A-}r_{B+}\rangle), \\ 2|v_{4\pm}\rangle &= |r_{B+}r_{A-}\rangle - |r_{A+}r_{B-}\rangle \pm (|r_{B-}r_{A+}\rangle - |r_{A-}r_{B+}\rangle). \end{aligned} \quad (\text{A19})$$

Note that the above result is valid for $\psi = 0$ or $\pi/2$. When $\psi = \pi/4$ or $3\pi/4$, there is an imaginary factor in the van der Waals interaction. Here the notations are defined as

$$\begin{aligned} \mathcal{V}_b &= \mathcal{V}_{11}, \quad \mathbb{V}_b = \mathbb{V}_{11} \\ \mathcal{V}_f &= \mathcal{V}_{14}, \quad \mathbb{V}_f = \mathbb{V}_{14}, \\ \mathcal{V}_d &= \mathcal{V}_{22}, \quad \mathbb{V}_d = \mathbb{V}_{22} \\ \mathcal{V}_e &= \mathcal{V}_{23}, \quad \mathbb{V}_e = \mathbb{V}_{23}. \end{aligned} \quad (\text{A20})$$

Obviously, $|v_{1\pm}/v_{2\pm}|, |v_{3\pm}/v_{4\pm}| \gg 1$ when $\Delta_A + \Delta_B = 0$.

(b) For the addressing of the same Rydberg level $n_A = 85$, one finds that the off-diagonal matrix elements of $\hat{H}_{\text{vdW}}^{(n_A, n_A)}$ in Eq. (A13) are more than 50 times smaller than the diagonal matrix elements. Thus we can ignore these off-diagonal matrix elements. Then diagonalization gives the following matrix:

$$\hat{H}^A = \text{diag}[\hat{H}_{\text{vdW}}^{(85,85)}] - 2\Delta_A \hat{1}_{4 \times 4}, \quad (\text{A21})$$

with the same basis vectors as in Eq. (A13). Similar results exist when we address the ground states to the same Rydberg level $n_A = 86$,

$$\hat{H}^B = \text{diag}[\hat{H}_{\text{vdW}}^{(86,86)}] - 2\Delta_B \hat{1}_{4 \times 4}. \quad (\text{A22})$$

With the diagonalization at hand, the unperturbed Hamiltonian for two atoms that are interacting with each other can be written as

$$\begin{aligned} \hat{H}_0 &= \sum_{\alpha=\pm, \beta=\uparrow, \downarrow} [-\Delta_A |r_{A\alpha}\beta\rangle \langle r_{A\alpha}\beta| - \Delta_B |r_{B\alpha}\beta\rangle \langle r_{B\alpha}\beta| \\ &\quad - \Delta_A |\beta r_{A\alpha}\rangle \langle \beta r_{A\alpha}| - \Delta_B |\beta r_{B\alpha}\rangle \langle \beta r_{B\alpha}|] \\ &\quad + \sum_{i=1}^4 \sum_{\alpha=\pm} E_{i\alpha} |v_{i\alpha}\rangle \langle v_{i\alpha}| + \hat{H}^A + \hat{H}^B. \end{aligned} \quad (\text{A23})$$

The perturbation in these basis can be written as

$$\begin{aligned} \hat{V} &= \frac{1}{2} \sum_i \sum_{\alpha=\pm, \beta} [\Omega_{A\alpha} e^{i\phi_{i\alpha}} |\uparrow\beta\rangle \langle r_{A\alpha}\beta| + \Omega_{B\alpha} e^{i\phi_{i\alpha}} |\downarrow\beta\rangle \langle r_{B\alpha}\beta| + \text{H.c.}] + \frac{1}{2} \sum_i \sum_{\alpha=\pm, \beta} [\Omega_{A\alpha} e^{i\phi_{2\alpha}} |\beta\uparrow\rangle \langle \beta r_{A\alpha}| \\ &\quad + \Omega_{B\alpha} e^{i\phi_{2\alpha}} |\beta\downarrow\rangle \langle \beta r_{B\alpha}| + \text{H.c.}], \end{aligned} \quad (\text{A24})$$

where the summation over β is for \uparrow, \downarrow and all the single Rydberg excited states. Let us write the above operator as

$$\hat{V} = \hat{V}_b + \hat{V}_o, \quad (\text{A25})$$

where

$$\begin{aligned} \hat{V}_0 = & \frac{1}{2} \sum_i \sum_{\alpha=\pm, \beta=\uparrow, \downarrow} [\Omega_{A\alpha} e^{i\phi_{1\alpha}} |\uparrow \beta\rangle \langle r_{A\alpha} \beta| + \Omega_{B\alpha} e^{i\phi_{1\alpha}} |\downarrow \beta\rangle \langle r_{B\alpha} \beta| + \text{H.c.}] + \frac{1}{2} \sum_i \sum_{\alpha=\pm, \beta=\uparrow, \downarrow} [\Omega_{A\alpha} e^{i\phi_{2\alpha}} |\beta \uparrow\rangle \langle \beta r_{A\alpha}| \\ & + \Omega_{B\alpha} e^{i\phi_{2\alpha}} |\beta \downarrow\rangle \langle \beta r_{B\alpha}| + \text{H.c.}], \end{aligned} \quad (\text{A26})$$

and $\hat{V}_b = \hat{V} - \hat{V}_0$. From Ref. [67], the unitary transformation $\hat{U} \equiv e^{\hat{G}}$ can get rid of the first-order coupling \hat{V} . \hat{G} shall be calculated order by order. According to this quasidegenerate perturbation theory, the goal of the perturbation is to eliminate the coupling \hat{V}_0 , so that the new ground states are decoupled from the excited states. In order to have the operator $\hat{U} \equiv e^{\hat{G}}$, where $\hat{G} = \sum_k \hat{G}^{(k)}$, one solves

$$\begin{aligned} [\hat{H}_0, \hat{G}^{(1)}] &= -\hat{V}_0, \\ [\hat{H}_0, \hat{G}^{(2)}] &= -[\hat{V}_b, \hat{G}^{(1)}], \\ [\hat{H}_0, \hat{G}^{(3)}] &= -[\hat{V}_b, \hat{G}^{(2)}] - \frac{1}{3} [[\hat{V}_0, \hat{G}^{(1)}], \hat{G}^{(1)}]. \end{aligned}$$

As an example, we solve

$$\begin{aligned} \hat{G}^{(1)} = & - \sum_{\alpha=\pm, \beta=\uparrow, \downarrow} \left[\frac{\Omega_{A\alpha} e^{i\phi_{1\alpha}}}{2\Delta_A} |\uparrow \beta\rangle \langle r_{A\alpha} \beta| + \frac{\Omega_{B\alpha} e^{i\phi_{1\alpha}}}{2\Delta_B} |\downarrow \beta\rangle \langle r_{B\alpha} \beta| - \text{H.c.} \right] \\ & - \sum_i \sum_{\alpha=\pm, \beta=\uparrow, \downarrow} \left[\frac{\Omega_{A\alpha} e^{i\phi_{2\alpha}}}{2\Delta_A} |\beta \uparrow\rangle \langle \beta r_{A\alpha}| + \frac{\Omega_{B\alpha} e^{i\phi_{2\alpha}}}{2\Delta_B} |\beta \downarrow\rangle \langle \beta r_{B\alpha}| - \text{H.c.} \right]. \end{aligned} \quad (\text{A27})$$

As soon as one gets $\hat{G}^{(1)}$, the second-order perturbed Hamiltonian is

$$\begin{aligned} \hat{H}_{\text{eff}}^{(2)} &= \frac{1}{2} [\hat{V}_0, \hat{G}^{(1)}] \\ &= \frac{\sum_{\alpha} \Omega_{A\alpha}^2}{2\Delta_A} |\uparrow \uparrow\rangle \langle \uparrow \uparrow| + \frac{\sum_{\alpha} \Omega_{B\alpha}^2}{2\Delta_B} |\downarrow \downarrow\rangle \langle \downarrow \downarrow| + \left(\frac{\sum_{\alpha} \Omega_{A\alpha}^2}{4\Delta_A} + \frac{\sum_{\alpha} \Omega_{B\alpha}^2}{4\Delta_B} \right) (|\uparrow \downarrow\rangle \langle \uparrow \downarrow| + |\downarrow \uparrow\rangle \langle \downarrow \uparrow|) \\ &\quad - \sum_{\alpha} \frac{\Omega_{A\alpha}^2}{4\Delta_A} \sum_{\beta=\downarrow, \uparrow} [|r_{A\alpha} \beta\rangle \langle r_{A\alpha} \beta| + |\beta r_{A\alpha}\rangle \langle \beta r_{A\alpha}|] - \sum_{\alpha} \frac{\Omega_{B\alpha}^2}{4\Delta_B} \sum_{\beta=\downarrow, \uparrow} [|r_{B\alpha} \beta\rangle \langle r_{B\alpha} \beta| + |\beta r_{B\alpha}\rangle \langle \beta r_{B\alpha}|], \end{aligned} \quad (\text{A28})$$

where one gets diagonal couplings within the excited states manifold. As long as we finally get rid of the coupling between the ground and excited states, we do not need to pay special attention to the energy levels of the excited states. We thence do so.

The calculation of the effective Hamiltonian can be conveniently performed following Ref. [68]. The third-order effective Hamiltonian is zero, while the result for fourth-order effective Hamiltonian is

$$\begin{aligned} \hat{H}_{\text{eff}}^{(4)} &= \frac{1}{2} [\hat{V}_0, \hat{G}^{(3)}] - \frac{1}{24} [[[\hat{V}_0, \hat{G}^{(1)}], \hat{G}^{(1)}], \hat{G}^{(1)}] \\ &= \hat{H}_{\text{light}}^{(4)} + \hat{H}_{\text{atom}}^{(4)}, \end{aligned} \quad (\text{A29})$$

where the part due to the laser field is

$$\begin{aligned} \hat{H}_{\text{light}}^{(4)} = & \left[-\frac{(\Omega_{A+}^2 + \Omega_{A-}^2)^2}{4\Delta_A^3} \right] |\uparrow \uparrow\rangle \langle \uparrow \uparrow| + \left[-\frac{(\Omega_{B+}^2 + \Omega_{B-}^2)^2}{4\Delta_B^3} \right] |\downarrow \downarrow\rangle \langle \downarrow \downarrow| \\ & - \left[\frac{(\Omega_{A+}^2 + \Omega_{A-}^2)^2}{16\Delta_A^3} + \frac{(\Omega_{B+}^2 + \Omega_{B-}^2)^2}{16\Delta_B^3} + \frac{(\Omega_{A+}^2 + \Omega_{A-}^2)(\Omega_{B+}^2 + \Omega_{B-}^2)}{16\Delta_A \Delta_B} \left(\frac{1}{\Delta_A} + \frac{1}{\Delta_B} \right) \right] (|\uparrow \downarrow\rangle \langle \uparrow \downarrow| + |\downarrow \uparrow\rangle \langle \downarrow \uparrow|) \\ & + \text{Energy shifts of excited states,} \end{aligned} \quad (\text{A30})$$

while the part due to Rydberg interaction is

$$\begin{aligned} \hat{H}_{\text{atom}}^{(4)} = & -\frac{1}{4\Delta_A^2} \sum_{\alpha, \beta=\pm} \frac{\Omega_{A\alpha}^2 \Omega_{A\beta}^2}{H_{\alpha\beta}^A} |\uparrow \uparrow\rangle \langle \uparrow \uparrow| - \frac{1}{4\Delta_B^2} \sum_{\alpha, \beta=\pm} \frac{\Omega_{B\alpha}^2 \Omega_{B\beta}^2}{H_{\alpha\beta}^B} |\downarrow \downarrow\rangle \langle \downarrow \downarrow| + \frac{1}{4} [h_1 + h_2 + h_3] (|\uparrow \downarrow\rangle \langle \uparrow \downarrow| + |\downarrow \uparrow\rangle \langle \downarrow \uparrow|) \\ & + \frac{1}{4} [(h_4 + h_5 + h_6) |\uparrow \downarrow\rangle \langle \downarrow \uparrow| + \text{H.c.}], \end{aligned} \quad (\text{A31})$$

where the calculation for the coefficient of $|\uparrow\downarrow\rangle\langle\uparrow\downarrow|$ can be done from Eq. (B15) of Ref. [68]. First, the contribution from $(|l\rangle, |l''\rangle) = (|r_{A\alpha}\downarrow\rangle, |r_{A\beta}\downarrow\rangle)$ is

$$\begin{aligned}
 h_1 = & -\frac{\Omega_{A+}^2\Omega_{B+}^2 + \Omega_{A-}^2\Omega_{B-}^2}{16\Delta_A^2} \sum_{k=1,2} \sum_{\alpha=\pm} \frac{1}{E_{k\alpha}} - \frac{\Omega_{A+}^2\Omega_{B-}^2 + \Omega_{A-}^2\Omega_{B+}^2}{16\Delta_A^2} \sum_{k=3,4} \sum_{\alpha=\pm} \frac{1}{E_{k\alpha}} \\
 & - \frac{\Omega_{A+}\Omega_{B+}\Omega_{A-}\Omega_{B-}}{8\Delta_A^2} \left(\frac{1}{E_{1+}} - \frac{1}{E_{1-}} + \frac{1}{E_{2+}} - \frac{1}{E_{2-}} \right) \cos(\phi_{1+} - \phi_{1-} + \varphi_{2+} - \varphi_{2-}) \\
 & - \frac{\Omega_{A+}\Omega_{B+}\Omega_{A-}\Omega_{B-}}{8\Delta_A^2} \left(\frac{1}{E_{3+}} - \frac{1}{E_{3-}} + \frac{1}{E_{4+}} - \frac{1}{E_{4-}} \right) \cos(\phi_{1+} - \phi_{1-} - \varphi_{2+} + \varphi_{2-}), \tag{A32}
 \end{aligned}$$

and the contribution from $(|l\rangle, |l''\rangle) = (|\uparrow r_{B\alpha}\rangle, |\uparrow r_{B\beta}\rangle)$ h_2 applies the same form as h_1 , but with Δ_A replaced by Δ_B . Now, the part from $(|l\rangle, |l''\rangle) = (|r_{A\alpha}\downarrow\rangle, |\uparrow r_{B\beta}\rangle)$ and $(|\uparrow r_{B\beta}\rangle, |r_{A\alpha}\downarrow\rangle)$ is

$$\begin{aligned}
 h_3 = & -\frac{\Omega_{A+}^2\Omega_{B+}^2 + \Omega_{A-}^2\Omega_{B-}^2}{8\Delta_A\Delta_B} \sum_{k=1,2} \sum_{\alpha=\pm} \frac{1}{E_{k\alpha}} - \frac{\Omega_{A+}^2\Omega_{B-}^2 + \Omega_{A-}^2\Omega_{B+}^2}{8\Delta_A\Delta_B} \sum_{k=3,4} \sum_{\alpha=\pm} \frac{1}{E_{k\alpha}} \\
 & - \frac{\Omega_{A+}\Omega_{B+}\Omega_{A-}\Omega_{B-}}{4\Delta_A\Delta_B} \left(\frac{1}{E_{1+}} - \frac{1}{E_{1-}} + \frac{1}{E_{2+}} - \frac{1}{E_{2-}} \right) \cos(\phi_{1+} - \phi_{1-} + \varphi_{2+} - \varphi_{2-}) \\
 & - \frac{\Omega_{A+}\Omega_{B+}\Omega_{A-}\Omega_{B-}}{4\Delta_A\Delta_B} \left(\frac{1}{E_{3+}} - \frac{1}{E_{3-}} + \frac{1}{E_{4+}} - \frac{1}{E_{4-}} \right) \cos(\phi_{1+} - \phi_{1-} - \varphi_{2+} + \varphi_{2-}). \tag{A33}
 \end{aligned}$$

We next come to the exchange part. The contribution from $(|l\rangle, |l''\rangle) = (|r_{A\alpha}\downarrow\rangle, |r_{B\beta}\uparrow\rangle)$ and $(|\uparrow r_{B\beta}\rangle, \downarrow r_{A\alpha})$ is

$$\begin{aligned}
 h_4 = & -\frac{1}{8\Delta_A\Delta_B} \sum_{\alpha} \left(\frac{1}{E_{1\alpha}} - \frac{1}{E_{2\alpha}} \right) [\Omega_{A+}^2\Omega_{B+}^2 \cos(\phi_{1+} - \phi_{2+} - \varphi_{1+} + \varphi_{2+}) + \Omega_{A-}^2\Omega_{B-}^2 \cos(\phi_{1-} - \phi_{2-} - \varphi_{1-} + \varphi_{2-})] \\
 & - \frac{\Omega_{A+}\Omega_{B+}\Omega_{A-}\Omega_{B-}}{8\Delta_A\Delta_B} \sum_{\alpha} \left(\frac{1}{E_{3\alpha}} - \frac{1}{E_{4\alpha}} \right) [\cos(\phi_{1+} - \phi_{2-} - \varphi_{1+} + \varphi_{2-}) + \cos(\phi_{1-} - \phi_{2+} - \varphi_{1-} + \varphi_{2+})] \\
 & - \frac{\Omega_{A+}\Omega_{B+}\Omega_{A-}\Omega_{B-}}{8\Delta_A\Delta_B} \sum_{\alpha} \left(\frac{\alpha}{E_{1\alpha}} - \frac{\alpha}{E_{2\alpha}} \right) [\cos(\phi_{1-} - \phi_{2+} - \varphi_{1+} + \varphi_{2-}) + \cos(\phi_{1+} - \phi_{2-} - \varphi_{1-} + \varphi_{2+})] \\
 & - \frac{1}{8\Delta_A\Delta_B} \sum_{\alpha} \left(\frac{\alpha}{E_{3\alpha}} - \frac{\alpha}{E_{4\alpha}} \right) [\Omega_{A+}^2\Omega_{B-}^2 \cos(\phi_{1+} - \phi_{2+} - \varphi_{1-} + \varphi_{2-}) + \Omega_{A-}^2\Omega_{B+}^2 \cos(\phi_{1-} - \phi_{2-} - \varphi_{1+} + \varphi_{2+})], \tag{A34}
 \end{aligned}$$

The contribution from $(|l\rangle, |l''\rangle) = (|r_{A\alpha}\downarrow\rangle, |\downarrow r_{A\beta}\rangle)$ is

$$\begin{aligned}
 h_5 = & -\frac{1}{16\Delta_A^2} \sum_{\alpha} \left(\frac{1}{E_{1\alpha}} - \frac{1}{E_{2\alpha}} \right) [\Omega_{A+}^2\Omega_{B+}^2 \exp[i(\phi_{1+} - \phi_{2+} - \varphi_{1+} + \varphi_{2+})] + \Omega_{A-}^2\Omega_{B-}^2 \exp[i(\phi_{1-} - \phi_{2-} - \varphi_{1-} + \varphi_{2-})]] \\
 & - \frac{\Omega_{A+}\Omega_{B+}\Omega_{A-}\Omega_{B-}}{16\Delta_A^2} \sum_{\alpha} \left(\frac{1}{E_{3\alpha}} - \frac{1}{E_{4\alpha}} \right) [\exp[i(\phi_{1+} - \phi_{2-} - \varphi_{1+} + \varphi_{2-})] + \exp[i(\phi_{1-} - \phi_{2+} - \varphi_{1-} + \varphi_{2+})]] \\
 & - \frac{\Omega_{A+}\Omega_{B+}\Omega_{A-}\Omega_{B-}}{16\Delta_A^2} \sum_{\alpha} \left(\frac{\alpha}{E_{1\alpha}} - \frac{\alpha}{E_{2\alpha}} \right) [\exp[i(\phi_{1-} - \phi_{2+} - \varphi_{1+} + \varphi_{2-})] + \exp[i(\phi_{1+} - \phi_{2-} - \varphi_{1-} + \varphi_{2+})]] \\
 & - \frac{1}{16\Delta_A^2} \sum_{\alpha} \left(\frac{\alpha}{E_{3\alpha}} - \frac{\alpha}{E_{4\alpha}} \right) [\Omega_{A+}^2\Omega_{B-}^2 \exp[i(\phi_{1+} - \phi_{2+} - \varphi_{1-} + \varphi_{2-})] + \Omega_{A-}^2\Omega_{B+}^2 \exp[i(\phi_{1-} - \phi_{2-} - \varphi_{1+} + \varphi_{2+})]]. \tag{A35}
 \end{aligned}$$

The contribution from $(|l\rangle, |l''\rangle) = (|\uparrow r_{B\alpha}\rangle, |r_{B\beta}\uparrow\rangle)$ is

$$\begin{aligned}
 h_6 = & -\frac{1}{16\Delta_B^2} \sum_{\alpha} \left(\frac{1}{E_{1\alpha}} - \frac{1}{E_{2\alpha}} \right) [\Omega_{A+}^2\Omega_{B+}^2 \exp[i(\phi_{1+} - \phi_{2+} - \varphi_{1+} + \varphi_{2+})] + \Omega_{A-}^2\Omega_{B-}^2 \exp[i(\phi_{1-} - \phi_{2-} - \varphi_{1-} + \varphi_{2-})]] \\
 & - \frac{\Omega_{A+}\Omega_{B+}\Omega_{A-}\Omega_{B-}}{16\Delta_B^2} \sum_{\alpha} \left(\frac{1}{E_{3\alpha}} - \frac{1}{E_{4\alpha}} \right) [\exp[i(\phi_{1+} - \phi_{2-} - \varphi_{1+} + \varphi_{2-})] + \exp[i(\phi_{1-} - \phi_{2+} - \varphi_{1-} + \varphi_{2+})]]
 \end{aligned}$$

$$\begin{aligned}
 & - \frac{\Omega_{A+}\Omega_{B+}\Omega_{A-}\Omega_{B-}}{16\Delta_B^2} \sum_{\alpha} \left(\frac{\alpha}{E_{1\alpha}} - \frac{\alpha}{E_{2\alpha}} \right) [\exp[i(\phi_{1-} - \phi_{2+} - \varphi_{1+} + \varphi_{2-})] + \exp[i(\phi_{1+} - \phi_{2-} - \varphi_{1-} + \varphi_{2+})]] \\
 & - \frac{1}{16\Delta_B^2} \sum_{\alpha} \left(\frac{\alpha}{E_{3\alpha}} - \frac{\alpha}{E_{4\alpha}} \right) [\Omega_{A+}^2 \Omega_{B-}^2 \exp[i(\phi_{1+} - \phi_{2+} - \varphi_{1-} + \varphi_{2-})] + \Omega_{A-}^2 \Omega_{B+}^2 \exp[i(\phi_{1-} - \phi_{2-} - \varphi_{1+} + \varphi_{2+})]].
 \end{aligned} \tag{A36}$$

In summary, the Hamiltonian up to fourth order for the two atoms i and j is

$$\hat{H}_{\text{eff}} = \hat{H}_0 + \hat{H}_{\text{eff}}^{(2)} + \hat{H}_{\text{eff}}^{(4)}. \tag{A37}$$

If L is so large that all van der Waals interaction is zero, \hat{H}_{eff} is still nonzero for the ground states,

$$\begin{aligned}
 \hat{H}_{\text{eff}} \rightarrow & \sum_{\alpha=\pm, \beta=\uparrow, \downarrow} [-\Delta_A |r_{A\alpha}\beta\rangle \langle r_{A\alpha}\beta| - \Delta_B |r_{B\alpha}\beta\rangle \langle r_{B\alpha}\beta| - \Delta_A |\beta r_{A\alpha}\rangle \langle \beta r_{A\alpha}| - \Delta_B |\beta r_{B\alpha}\rangle \langle \beta r_{B\alpha}|] \\
 & + \sum_{k=1}^4 \sum_{\alpha=\pm} E_{k\alpha} |v_{k\alpha}\rangle \langle v_{k\alpha}| + \hat{H}^A + \hat{H}^B \\
 & + h_{\text{light}} + \text{energy shifts of excited states,}
 \end{aligned} \tag{A38}$$

where one finds the light shift of the ground states

$$\begin{aligned}
 h_{\text{light}} = & \frac{\sum_{\alpha} \Omega_{A\alpha}^2}{2\Delta_A} |\uparrow\uparrow\rangle \langle \uparrow\uparrow| + \frac{\sum_{\alpha} \Omega_{B\alpha}^2}{2\Delta_B} |\downarrow\downarrow\rangle \langle \downarrow\downarrow| + \left(\frac{\sum_{\alpha} \Omega_{A\alpha}^2}{4\Delta_A} + \frac{\sum_{\alpha} \Omega_{B\alpha}^2}{4\Delta_B} \right) (|\uparrow\downarrow\rangle \langle \uparrow\downarrow| + |\downarrow\uparrow\rangle \langle \downarrow\uparrow|) \\
 & - \frac{(\Omega_{A+}^2 + \Omega_{A-}^2)^2}{8\Delta_A^3} |\uparrow\uparrow\rangle \langle \uparrow\uparrow| - \frac{(\Omega_{B+}^2 + \Omega_{B-}^2)^2}{8\Delta_B^3} |\downarrow\downarrow\rangle \langle \downarrow\downarrow| \\
 & - \left[\frac{(\Omega_{A+}^2 + \Omega_{A-}^2)^2}{16\Delta_A^3} + \frac{(\Omega_{B+}^2 + \Omega_{B-}^2)^2}{16\Delta_B^3} \right] (|\uparrow\downarrow\rangle \langle \uparrow\downarrow| + |\downarrow\uparrow\rangle \langle \downarrow\uparrow|).
 \end{aligned} \tag{A39}$$

The term h_{light} shows that detuning of the states are changed effectively to be

$$\begin{aligned}
 |r_{A\alpha}\rangle : & \Delta_A + \frac{\sum_{\alpha} \Omega_{A\alpha}^2}{4\Delta_A} - \frac{(\Omega_{A+}^2 + \Omega_{A-}^2)^2}{16\Delta_A^3} + \text{shifts due to excited states,} \\
 |r_{B\alpha}\rangle : & \Delta_B + \frac{\sum_{\alpha} \Omega_{B\alpha}^2}{4\Delta_B} - \frac{(\Omega_{B+}^2 + \Omega_{B-}^2)^2}{16\Delta_B^3} + \text{shifts due to excited states.}
 \end{aligned} \tag{A40}$$

As a result, the effective Hamiltonian can be written as

$$\begin{aligned}
 \hat{H}_{\text{eff}} = & [\hat{H}_0 + \hat{H}_{\text{eff}}^{(2)} + \hat{H}_{\text{eff}}^{(4)} - h_{\text{light}}]_{\text{ground states}} \\
 = & \mathbf{H}_{11} |\uparrow\uparrow\rangle \langle \uparrow\uparrow| + \mathbf{H}_{44} |\downarrow\downarrow\rangle \langle \downarrow\downarrow| \\
 & + \mathbf{H}_{22} (|\uparrow\downarrow\rangle \langle \uparrow\downarrow| + |\downarrow\uparrow\rangle \langle \downarrow\uparrow|) + \mathbf{H}_{23}^* |\uparrow\downarrow\rangle \langle \downarrow\uparrow| + \mathbf{H}_{23} |\downarrow\uparrow\rangle \langle \uparrow\downarrow|.
 \end{aligned} \tag{A41}$$

Here

$$\begin{aligned}
 \mathbf{H}_{11} = & - \frac{(\Omega_{A+}^2 + \Omega_{A-}^2)^2}{8\Delta_A^3} - \frac{1}{4\Delta_A^2} \sum_{\alpha, \beta=\pm} \frac{\Omega_{A\alpha}^2 \Omega_{A\beta}^2}{H_{\alpha\beta}^A}, \\
 \mathbf{H}_{44} = & - \frac{(\Omega_{B+}^2 + \Omega_{B-}^2)^2}{8\Delta_B^3} - \frac{1}{4\Delta_B^2} \sum_{\alpha, \beta=\pm} \frac{\Omega_{B\alpha}^2 \Omega_{B\beta}^2}{H_{\alpha\beta}^B}, \\
 \mathbf{H}_{22} = & - \frac{(\Omega_{A+}^2 + \Omega_{A-}^2)(\Omega_{B+}^2 + \Omega_{B-}^2)}{16\Delta_A \Delta_B} \left(\frac{1}{\Delta_A} + \frac{1}{\Delta_B} \right) \\
 & + \left(\frac{1}{\Delta_A} + \frac{1}{\Delta_B} \right)^2 \left[- \frac{\Omega_{A+}^2 \Omega_{B+}^2 + \Omega_{A-}^2 \Omega_{B-}^2}{16} \sum_{k=1,2} \sum_{\alpha=\pm} \frac{1}{E_{k\alpha}} - \frac{\Omega_{A+}^2 \Omega_{B-}^2 + \Omega_{A-}^2 \Omega_{B+}^2}{16} \sum_{k=3,4} \sum_{\alpha=\pm} \frac{1}{E_{k\alpha}} \right. \\
 & \left. - \frac{\Omega_{A+}\Omega_{B+}\Omega_{A-}\Omega_{B-}}{8} \left(\frac{1}{E_{1+}} - \frac{1}{E_{1-}} + \frac{1}{E_{2+}} - \frac{1}{E_{2-}} \right) \cos(\phi_{1+} - \phi_{1-} + \varphi_{2+} - \varphi_{2-}) \right]
 \end{aligned}$$

$$\begin{aligned}
 & - \frac{\Omega_{A+}\Omega_{B+}\Omega_{A-}\Omega_{B-}}{8} \left(\frac{1}{E_{3+}} - \frac{1}{E_{3-}} + \frac{1}{E_{4+}} - \frac{1}{E_{4-}} \right) \cos(\phi_{1+} - \phi_{1-} - \phi_{2+} + \phi_{2-}) \Big], \\
 \mathbf{H}_{23} &= h_4 + h_5 + h_6, \\
 \text{ReH}_{23} &= \left\{ -\frac{1}{16} \sum_{\alpha} \left(\frac{1}{E_{1\alpha}} - \frac{1}{E_{2\alpha}} \right) [\Omega_{A+}^2 \Omega_{B+}^2 \cos(\phi_{1+} - \phi_{2+} - \phi_{1+} + \phi_{2+}) + \Omega_{A-}^2 \Omega_{B-}^2 \cos(\phi_{1-} - \phi_{2-} - \phi_{1-} + \phi_{2-})] \right. \\
 & - \frac{\Omega_{A+}\Omega_{B+}\Omega_{A-}\Omega_{B-}}{16} \sum_{\alpha} \left(\frac{1}{E_{3\alpha}} - \frac{1}{E_{4\alpha}} \right) [\cos(\phi_{1+} - \phi_{2-} - \phi_{1+} + \phi_{2-}) + \cos(\phi_{1-} - \phi_{2+} - \phi_{1-} + \phi_{2+})] \\
 & - \frac{\Omega_{A+}\Omega_{B+}\Omega_{A-}\Omega_{B-}}{16} \sum_{\alpha} \left(\frac{\alpha}{E_{1\alpha}} - \frac{\alpha}{E_{2\alpha}} \right) [\cos(\phi_{1-} - \phi_{2+} - \phi_{1+} + \phi_{2-}) + \cos(\phi_{1+} - \phi_{2-} - \phi_{1-} + \phi_{2+})] \\
 & \left. - \frac{1}{16} \sum_{\alpha} \left(\frac{\alpha}{E_{3\alpha}} - \frac{\alpha}{E_{4\alpha}} \right) [\Omega_{A+}^2 \Omega_{B-}^2 \cos(\phi_{1+} - \phi_{2+} - \phi_{1-} + \phi_{2-}) + \Omega_{A-}^2 \Omega_{B+}^2 \cos(\phi_{1-} - \phi_{2-} - \phi_{1+} + \phi_{2+})] \right\} \\
 & \times \left(\frac{1}{\Delta_A} + \frac{1}{\Delta_B} \right)^2, \\
 \text{ImH}_{23} &= \left\{ -\frac{1}{16} \sum_{\alpha} \left(\frac{1}{E_{1\alpha}} - \frac{1}{E_{2\alpha}} \right) [\Omega_{A+}^2 \Omega_{B+}^2 \sin(\phi_{1+} - \phi_{2+} - \phi_{1+} + \phi_{2+}) + \Omega_{A-}^2 \Omega_{B-}^2 \sin(\phi_{1-} - \phi_{2-} - \phi_{1-} + \phi_{2-})] \right. \\
 & - \frac{\Omega_{A+}\Omega_{B+}\Omega_{A-}\Omega_{B-}}{16} \sum_{\alpha} \left(\frac{1}{E_{3\alpha}} - \frac{1}{E_{4\alpha}} \right) [\sin(\phi_{1+} - \phi_{2-} - \phi_{1+} + \phi_{2-}) + \sin(\phi_{1-} - \phi_{2+} - \phi_{1-} + \phi_{2+})] \\
 & - \frac{\Omega_{A+}\Omega_{B+}\Omega_{A-}\Omega_{B-}}{16} \sum_{\alpha} \left(\frac{\alpha}{E_{1\alpha}} - \frac{\alpha}{E_{2\alpha}} \right) [\sin(\phi_{1-} - \phi_{2+} - \phi_{1+} + \phi_{2-}) + \sin(\phi_{1+} - \phi_{2-} - \phi_{1-} + \phi_{2+})] \\
 & \left. - \frac{1}{16} \sum_{\alpha} \left(\frac{\alpha}{E_{3\alpha}} - \frac{\alpha}{E_{4\alpha}} \right) [\Omega_{A+}^2 \Omega_{B-}^2 \sin(\phi_{1+} - \phi_{2+} - \phi_{1-} + \phi_{2-}) + \Omega_{A-}^2 \Omega_{B+}^2 \sin(\phi_{1-} - \phi_{2-} - \phi_{1+} + \phi_{2+})] \right\} \\
 & \times \left(\frac{1}{\Delta_A} + \frac{1}{\Delta_B} \right)^2. \tag{A42}
 \end{aligned}$$

The result above can be written in terms of Pauli matrices $\hat{\sigma}_z^{(i)} \equiv 2|\uparrow\rangle\langle\uparrow|_i - \hat{1}^{(i)} = \hat{1}^{(i)} - 2|\downarrow\rangle\langle\downarrow|_i$, $\hat{\sigma}_x^{(i)} \equiv |\uparrow\rangle\langle\downarrow|_i + |\downarrow\rangle\langle\uparrow|_i$, and $\hat{\sigma}_y^{(i)} \equiv i|\downarrow\rangle\langle\uparrow|_i - i|\uparrow\rangle\langle\downarrow|_i$, with $\hat{1}^{(i)}$ the identity operator in the Hilbert space of the the two spin states of the i th atom,

$$\hat{H} = \sum_i B_i \hat{\sigma}_z^{(i)} / 2 + \sum_{\langle i,j \rangle} \sum_{\alpha=x,y,z} J_{\alpha\alpha} \hat{\sigma}_{\alpha}^{(i)} \hat{\sigma}_{\alpha}^{(j)} / 4 + \sum_{\langle i,j \rangle} (J_{xy} \hat{\sigma}_x^{(i)} \hat{\sigma}_y^{(j)} + J_{yx} \hat{\sigma}_y^{(i)} \hat{\sigma}_x^{(j)}) / 4, \tag{A43}$$

where

$$\begin{aligned}
 B_i &= \sum_j [\mathbf{H}_{11} - \mathbf{H}_{44}]_{i,j} / 2, \\
 J_{xx} &= J_{yy} = 2\text{ReH}_{23}, \\
 J_{zz} &= \mathbf{H}_{11} - 2\mathbf{H}_{22} + \mathbf{H}_{44}, \\
 J_{xy} &= -J_{yx} = 2\text{ImH}_{23}. \tag{A44}
 \end{aligned}$$

Now the hard-core boson is defined as $b_i^{\dagger} = |\uparrow\rangle\langle\downarrow|_i$, then $\hat{\sigma}_x^{(i)} = b_i^{\dagger} + b_i$, $\hat{\sigma}_y^{(i)} = i(b_i - b_i^{\dagger})$ and $\hat{\sigma}_z^{(i)} = 2b_i^{\dagger} b_i - 1$. Thus we have

$$\hat{H} = \sum_i \mu_i n_i + \sum_{\langle i,j \rangle} t_{ij} b_i^{\dagger} b_j + \sum_{\langle i,j \rangle} V_{ij} n_i n_j, \tag{A45}$$

where $n_i = b_i^{\dagger} b_i$, and

$$\begin{aligned}
 \mu_i &= B_i - \sum_j [J_{zz}]_{i,j} / 2 = \sum_j [\mathbf{H}_{22} - \mathbf{H}_{44}]_{i,j}, \\
 t_{ij} &= (J_{xx} + iJ_{xy}) / 2 = \mathbf{H}_{23}, \\
 V_{ij} &= J_{zz} = \mathbf{H}_{11} - 2\mathbf{H}_{22} + \mathbf{H}_{44}. \tag{A46}
 \end{aligned}$$

Note that if we have $H_{33} \neq H_{22}$, then

$$\begin{aligned}\mu_i &= B_i - \sum_j [J_{zz}]_{i,j}/2 = \sum_j [H_{22} + H_{33} - 2H_{44}]_{i,j}/2, \\ t_{ij} &= (J_{xx} + iJ_{xy})/2 = H_{23}, \\ V_{ij} &= J_{zz} = H_{11} - H_{22} - H_{33} + H_{44}.\end{aligned}\quad (\text{A47})$$

The above derivation shows that the wrong polarization of the laser fields will lead to fourth-order terms that are of order $\Omega_{i-}\Omega_{j-}/(\Omega_{i'+}\Omega_{j'+})$, where i, j, i', j' are A or B. This means that with a polarization purity 10^4 which leads to $\Omega_{i-}/\Omega_{i'+}, \Omega_{j-}/\Omega_{j'+} \sim 0.01$, the extra terms in the fourth-order are about 10^{-4} times the terms relevant for the topological order to appear, so that the wrong excitation channels can be ignored.

3. Boson-Harburg model on a honeycomb lattice

We use six types of Rydberg levels for the model. The state ($|\uparrow\rangle, |\downarrow\rangle$) for each site of sublattice a in the honeycomb lattice of Fig. 1(a) is excited to Rydberg states $(n_A S_{1/2}, n_B S_{1/2})$ and $(n_C S_{1/2}, n_D S_{1/2})$, while each site of sublattice b is excited to Rydberg states $(n_A S_{1/2}, n_B S_{1/2})$ and $(n_E S_{1/2}, n_F S_{1/2})$. The blockade interaction happens between two atoms of any Rydberg levels, while n -exchange interaction occurs only for pairs of levels $(n_A S_{1/2}, n_B S_{1/2})$, $(n_C S_{1/2}, n_D S_{1/2})$, or $(n_E S_{1/2}, n_F S_{1/2})$. The intermediate P levels for addressing $(n_C S_{1/2}, n_D S_{1/2})$ and $(n_E S_{1/2}, n_F S_{1/2})$ are chosen to have $F = 1$ and $F = 2$, respectively. We will apply the analytical result in the last section for levels $(n_A S_{1/2}, n_B S_{1/2})$, set Ω_{A-} and Ω_{B-} as zero, and ignore the populations on the Rydberg states $|r_{A-}\rangle, |r_{B-}\rangle$. We use Ω_A for Ω_{A+} below, and similarly for others. The same symbols are applied for levels $(n_C S_{1/2}, n_D S_{1/2})$ and $(n_E S_{1/2}, n_F S_{1/2})$, with the subscripts replaced correspondingly. For $|n_\alpha - n_\beta| \neq 1$, the interaction for levels $(n_\alpha S_{1/2}, n_\beta S_{1/2})$ is only an energy shift, which is represented by $V^{(n_\alpha, n_\beta)}$. For two nearest atoms in sublattice a, the coefficients in Eq. (A42) becomes

$$\begin{aligned}H_{11}^{(aa)} &= -\frac{\Omega_A^4}{8\Delta_A^3} - \frac{\Omega_C^4}{8\Delta_C^3} - \frac{\Omega_A^2\Omega_C^2(1/\Delta_A^2 + 1/\Delta_C^2)}{4(\Delta_A + \Delta_C)} - \frac{1}{4} \left[\frac{\Omega_A^2\Omega_A^2/\Delta_A^2}{V^{(n_A, n_A)} - 2\Delta_A} + \frac{\Omega_A^2\Omega_C^2(1/\Delta_A^2 + 1/\Delta_C^2)}{V^{(n_A, n_C)} - \Delta_A - \Delta_C} + \frac{\Omega_C^2\Omega_C^2/\Delta_C^2}{V^{(n_C, n_C)} - 2\Delta_C} \right], \\ H_{44}^{(aa)} &= -\frac{\Omega_B^4}{8\Delta_B^3} - \frac{\Omega_D^4}{8\Delta_D^3} - \frac{\Omega_B^2\Omega_D^2(1/\Delta_B^2 + 1/\Delta_D^2)}{4(\Delta_B + \Delta_D)} - \frac{1}{4} \left[\frac{\Omega_B^2\Omega_B^2/\Delta_B^2}{V^{(n_B, n_B)} - 2\Delta_B} + \frac{\Omega_B^2\Omega_D^2(1/\Delta_B^2 + 1/\Delta_D^2)}{V^{(n_B, n_D)} - \Delta_B - \Delta_D} + \frac{\Omega_D^2\Omega_D^2/\Delta_D^2}{V^{(n_D, n_D)} - 2\Delta_D} \right], \\ H_{22}^{(aa)} &= -\frac{\Omega_A^2\Omega_B^2(1/\Delta_A + 1/\Delta_B)}{16\Delta_A\Delta_B} - \frac{\Omega_A^2\Omega_D^2(1/\Delta_A + 1/\Delta_D)}{16\Delta_A\Delta_D} - \frac{\Omega_C^2\Omega_B^2(1/\Delta_C + 1/\Delta_B)}{16\Delta_C\Delta_B} - \frac{\Omega_C^2\Omega_D^2(1/\Delta_C + 1/\Delta_D)}{16\Delta_C\Delta_D} \\ &\quad - \left(\frac{1}{\Delta_A} + \frac{1}{\Delta_B} \right)^2 \sum_{\beta=\pm} \frac{\Omega_A^2\Omega_B^2}{32(-\Delta_A - \Delta_B + \mathcal{V}_b^{(n_A, n_B)} + \beta\mathbb{V}_b^{(n_A, n_B)})} \\ &\quad - \left(\frac{1}{\Delta_C} + \frac{1}{\Delta_D} \right)^2 \sum_{\beta=\pm} \frac{\Omega_C^2\Omega_D^2}{32(-\Delta_C - \Delta_D + \mathcal{V}_b^{(n_C, n_D)} + \beta\mathbb{V}_b^{(n_C, n_D)})} \\ &\quad - \left(\frac{1}{\Delta_A} + \frac{1}{\Delta_D} \right)^2 \frac{\Omega_A^2\Omega_D^2}{16(-\Delta_A - \Delta_D + V^{(n_A, n_D)})} - \left(\frac{1}{\Delta_C} + \frac{1}{\Delta_B} \right)^2 \frac{\Omega_B^2\Omega_C^2}{16(-\Delta_C - \Delta_B + V^{(n_B, n_C)})}, \\ \text{Re}H_{23}^{(aa)} &= -\left(\frac{1}{\Delta_A} + \frac{1}{\Delta_B} \right)^2 \sum_{\beta=\pm} \frac{\beta\Omega_A^2\Omega_B^2[\cos(\phi_{1+} - \phi_{2+} - \varphi_{1+} + \varphi_{2+})]^{(n_A, n_B)}}{32(-\Delta_A - \Delta_B + \mathcal{V}_b^{(n_A, n_B)} + \beta\mathbb{V}_b^{(n_A, n_B)})} \\ &\quad - \left(\frac{1}{\Delta_C} + \frac{1}{\Delta_D} \right)^2 \sum_{\beta=\pm} \frac{\beta\Omega_C^2\Omega_D^2[\cos(\phi_{1+} - \phi_{2+} - \varphi_{1+} + \varphi_{2+})]^{(n_C, n_D)}}{32(-\Delta_C - \Delta_D + \mathcal{V}_b^{(n_C, n_D)} + \beta\mathbb{V}_b^{(n_C, n_D)})}, \\ \text{Im}H_{23}^{(aa)} &= -\left(\frac{1}{\Delta_A} + \frac{1}{\Delta_B} \right)^2 \sum_{\beta=\pm} \frac{\beta\Omega_A^2\Omega_B^2[\sin(\phi_{1+} - \phi_{2+} - \varphi_{1+} + \varphi_{2+})]^{(n_A, n_B)}}{32(-\Delta_A - \Delta_B + \mathcal{V}_b^{(n_A, n_B)} + \beta\mathbb{V}_b^{(n_A, n_B)})} \\ &\quad - \left(\frac{1}{\Delta_C} + \frac{1}{\Delta_D} \right)^2 \sum_{\beta=\pm} \frac{\beta\Omega_C^2\Omega_D^2[\sin(\phi_{1+} - \phi_{2+} - \varphi_{1+} + \varphi_{2+})]^{(n_C, n_D)}}{32(-\Delta_C - \Delta_D + \mathcal{V}_b^{(n_C, n_D)} + \beta\mathbb{V}_b^{(n_C, n_D)})}.\end{aligned}\quad (\text{A48})$$

For two nearest atoms in sublattice b, the coefficients are in the same form of Eq. (A48), with C, D replaced by E, F . For convenience, the next-nearest-neighboring hopping on sublattice a is divided into two parts, t_{NN} that carries no phase and $t_{\text{NN}}^{(aa)}$ that carries a phase, and similarly for that on sublattice b.

For two nearest atoms, one at sublattice a, the other on b, the effective Hamiltonian is

$$\begin{aligned} \hat{H}_{\text{eff}} &= [\hat{H}_0 + \hat{H}_{\text{eff}}^{(2)} + \hat{H}_{\text{eff}}^{(4)} - h_{\text{light}}]_{\text{ground states}} \\ &= \mathbf{H}_{11}^{(ab)} |\uparrow\uparrow\rangle\langle\uparrow\uparrow| + \mathbf{H}_{44}^{(ab)} |\downarrow\downarrow\rangle\langle\downarrow\downarrow| + \mathbf{H}_{22}^{(ab)} |\uparrow\downarrow\rangle\langle\uparrow\downarrow| + \mathbf{H}_{33}^{(ab)} |\downarrow\uparrow\rangle\langle\downarrow\uparrow| + \mathbf{H}_{23}^{(ab)} |\uparrow\downarrow\rangle\langle\downarrow\uparrow| + \mathbf{H}_{23}^{(ab)*} |\downarrow\uparrow\rangle\langle\uparrow\downarrow|, \end{aligned} \quad (\text{A49})$$

where one finds that \mathbf{H}_{22} differs from \mathbf{H}_{33} . In detail,

$$\begin{aligned} \mathbf{H}_{11}^{(ab)} &= -\frac{\Omega_A^4}{8\Delta_A^3} - \frac{\Omega_A^2\Omega_C^2(1/\Delta_A^2 + 1/\Delta_C^2)}{8(\Delta_A + \Delta_C)} - \frac{\Omega_A^2\Omega_E^2(1/\Delta_A^2 + 1/\Delta_E^2)}{8(\Delta_A + \Delta_E)} - \frac{\Omega_C^2\Omega_E^2(1/\Delta_C^2 + 1/\Delta_E^2)}{8(\Delta_C + \Delta_E)} \\ &\quad - \frac{1}{4} \frac{\Omega_A^2\Omega_A^2/\Delta_A^2}{V^{(n_A, n_A)} - 2\Delta_A} - \frac{1}{8} \frac{\Omega_A^2\Omega_C^2(1/\Delta_A^2 + 1/\Delta_C^2)}{V^{(n_A, n_C)} - \Delta_A - \Delta_C} - \frac{1}{8} \frac{\Omega_A^2\Omega_E^2(1/\Delta_A^2 + 1/\Delta_E^2)}{V^{(n_A, n_E)} - \Delta_A - \Delta_E} - \frac{1}{8} \frac{\Omega_C^2\Omega_E^2(1/\Delta_C^2 + 1/\Delta_E^2)}{V^{(n_C, n_E)} - \Delta_C - \Delta_E}, \\ \mathbf{H}_{44}^{(ab)} &= -\frac{\Omega_B^4}{8\Delta_B^3} - \frac{\Omega_B^2\Omega_D^2(1/\Delta_B^2 + 1/\Delta_D^2)}{8(\Delta_B + \Delta_D)} - \frac{\Omega_B^2\Omega_F^2(1/\Delta_B^2 + 1/\Delta_F^2)}{8(\Delta_B + \Delta_F)} - \frac{\Omega_D^2\Omega_F^2(1/\Delta_D^2 + 1/\Delta_F^2)}{8(\Delta_D + \Delta_F)} \\ &\quad - \frac{1}{4} \frac{\Omega_B^2\Omega_B^2/\Delta_B^2}{V^{(n_B, n_B)} - 2\Delta_B} - \frac{1}{8} \frac{\Omega_B^2\Omega_D^2(1/\Delta_B^2 + 1/\Delta_D^2)}{V^{(n_B, n_D)} - \Delta_B - \Delta_D} - \frac{1}{8} \frac{\Omega_B^2\Omega_F^2(1/\Delta_B^2 + 1/\Delta_F^2)}{V^{(n_B, n_F)} - \Delta_B - \Delta_F} - \frac{1}{8} \frac{\Omega_D^2\Omega_F^2(1/\Delta_D^2 + 1/\Delta_F^2)}{V^{(n_D, n_F)} - \Delta_D - \Delta_F}, \\ \mathbf{H}_{22}^{(ab)} &= -\frac{\Omega_A^2\Omega_B^2(1/\Delta_A + 1/\Delta_B)}{16\Delta_A\Delta_B} - \frac{\Omega_A^2\Omega_F^2(1/\Delta_A + 1/\Delta_F)}{16\Delta_A\Delta_F} - \frac{\Omega_C^2\Omega_B^2(1/\Delta_C + 1/\Delta_B)}{16\Delta_C\Delta_B} - \frac{\Omega_C^2\Omega_F^2(1/\Delta_C + 1/\Delta_F)}{16\Delta_C\Delta_F} \\ &\quad - \left(\frac{1}{\Delta_A} + \frac{1}{\Delta_B}\right)^2 \sum_{\beta=\pm} \frac{\Omega_A^2\Omega_B^2}{32(-\Delta_A - \Delta_B + \mathcal{V}_b^{(n_A, n_B)} + \beta\mathbb{V}_b^{(n_A, n_B)})} \\ &\quad - \left(\frac{1}{\Delta_C} + \frac{1}{\Delta_F}\right)^2 \frac{\Omega_C^2\Omega_F^2}{16(-\Delta_C - \Delta_F + V^{(n_C, n_F)})} \\ &\quad - \left(\frac{1}{\Delta_A} + \frac{1}{\Delta_F}\right)^2 \frac{\Omega_A^2\Omega_F^2}{16(-\Delta_A - \Delta_F + V^{(n_A, n_F)})} - \left(\frac{1}{\Delta_C} + \frac{1}{\Delta_B}\right)^2 \frac{\Omega_B^2\Omega_C^2}{16(-\Delta_C - \Delta_B + V^{(n_B, n_C)})}, \\ \mathbf{H}_{33}^{(ab)} &= -\frac{\Omega_A^2\Omega_B^2(1/\Delta_A + 1/\Delta_B)}{16\Delta_A\Delta_B} - \frac{\Omega_A^2\Omega_D^2(1/\Delta_A + 1/\Delta_D)}{16\Delta_A\Delta_D} - \frac{\Omega_E^2\Omega_B^2(1/\Delta_E + 1/\Delta_B)}{16\Delta_E\Delta_B} - \frac{\Omega_E^2\Omega_D^2(1/\Delta_E + 1/\Delta_D)}{16\Delta_E\Delta_D} \\ &\quad - \left(\frac{1}{\Delta_A} + \frac{1}{\Delta_B}\right)^2 \sum_{\beta=\pm} \frac{\Omega_A^2\Omega_B^2}{32(-\Delta_A - \Delta_B + \mathcal{V}_b^{(n_A, n_B)} + \beta\mathbb{V}_b^{(n_A, n_B)})} \\ &\quad - \left(\frac{1}{\Delta_E} + \frac{1}{\Delta_D}\right)^2 \frac{\Omega_E^2\Omega_D^2}{16(-\Delta_E - \Delta_D + V^{(n_E, n_D)})} \\ &\quad - \left(\frac{1}{\Delta_A} + \frac{1}{\Delta_D}\right)^2 \frac{\Omega_A^2\Omega_D^2}{16(-\Delta_A - \Delta_D + V^{(n_A, n_D)})} - \left(\frac{1}{\Delta_E} + \frac{1}{\Delta_B}\right)^2 \frac{\Omega_B^2\Omega_E^2}{16(-\Delta_E - \Delta_B + V^{(n_B, n_E)})}, \\ \text{ReH}_{23}^{(ab)} &= -\left(\frac{1}{\Delta_A} + \frac{1}{\Delta_B}\right)^2 \sum_{\beta=\pm} \frac{\beta\Omega_A^2\Omega_B^2[\cos(\phi_{1+} - \phi_{2+} - \varphi_{1+} + \varphi_{2+})]^{(n_A, n_B)}}{32(-\Delta_A - \Delta_B + \mathcal{V}_b^{(n_A, n_B)} + \beta\mathbb{V}_b^{(n_A, n_B)})}, \\ \text{ImH}_{23}^{(ab)} &= -\left(\frac{1}{\Delta_A} + \frac{1}{\Delta_B}\right)^2 \sum_{\beta=\pm} \frac{\beta\Omega_A^2\Omega_B^2[\sin(\phi_{1+} - \phi_{2+} - \varphi_{1+} + \varphi_{2+})]^{(n_A, n_B)}}{32(-\Delta_A - \Delta_B + \mathcal{V}_b^{(n_A, n_B)} + \beta\mathbb{V}_b^{(n_A, n_B)})}. \end{aligned} \quad (\text{A50})$$

Thus the two-dimensional model on a honeycomb lattice has the following Hamiltonian:

$$\hat{H} = \sum_i \mu_i n_i + \sum_{(i,j)} t_{ij} b_i^\dagger b_j + \sum_{(i,j)} V_{ij} n_i n_j, \quad (\text{A51})$$

where $n_i = b_i^\dagger b_i$, and for i on sublattice a,

$$\begin{aligned} \mu_i &= \sum_j [\mathbf{H}_{22} - \mathbf{H}_{44}]_{i,j} = \sum_j [\mathbf{H}_{22}^{(aa)} - \mathbf{H}_{44}^{(aa)}]_{i,j} + \sum_j [\mathbf{H}_{22}^{(ab)} - \mathbf{H}_{44}^{(ab)}]_{i,j}, \\ V_{ij}^{(aa)} &= \mathbf{H}_{11}^{(aa)} + \mathbf{H}_{44}^{(aa)} - [\mathbf{H}_{22}^{(aa)} + \mathbf{H}_{33}^{(aa)}], \\ V_{ij}^{(ab)} &= \mathbf{H}_{11}^{(ab)} + \mathbf{H}_{44}^{(ab)} - [\mathbf{H}_{22}^{(ab)} + \mathbf{H}_{33}^{(ab)}], \end{aligned} \quad (\text{A52})$$

and similarly for i on sublattice b. Note that when calculating μ_i , each site has six next-nearest neighbors and three nearest neighbors. For i and j on sublattice a and b, or the same sublattice, we have

$$t_{ij}^{(ab)} = H_{23}^{(ab)}, t_{ij}^{(aa)} = H_{23}^{(aa)}, t_{ij}^{(bb)} = H_{23}^{(bb)}. \quad (\text{A53})$$

The phase terms arise due to laser phases. The nearest atoms have distance $L = 12.8 \mu\text{m}$. For each site of the honeycomb lattice in Fig. 1(a), let us show how the phase term can be calculated when states $|\uparrow\rangle$ and $|\downarrow\rangle$ are addressed to states $|r_{A+}\rangle$ and $|r_{B+}\rangle$ via intermediate states $5P_{3/2}$. We calculate the phase terms according to Ref. [81] about the setup in Fig. 1. For two atoms labeled as 1 and 2,

$$\begin{aligned} \phi_{1+} &= (\mathbf{k}_{5S_{1/2}, F=1 \rightarrow 5P_{3/2}} + \mathbf{K}_{5P_{3/2} \rightarrow n_A S_{1/2}}) \cdot \mathbf{r}_1, \\ \varphi_{1+} &= (\mathbf{k}_{5S_{1/2}, F=2 \rightarrow 5P_{3/2}} + \mathbf{K}'_{5P_{3/2} \rightarrow n_B S_{1/2}}) \cdot \mathbf{r}_1, \\ \phi_{2+} &= (\mathbf{k}_{5S_{1/2}, F=1 \rightarrow 5P_{3/2}} + \mathbf{K}_{5P_{3/2} \rightarrow n_A S_{1/2}}) \cdot \mathbf{r}_2, \\ \varphi_{2+} &= (\mathbf{k}_{5S_{1/2}, F=2 \rightarrow 5P_{3/2}} + \mathbf{K}'_{5P_{3/2} \rightarrow n_B S_{1/2}}) \cdot \mathbf{r}_2, \end{aligned} \quad (\text{A54})$$

where we have ignored the detunings of the laser, since it is negligible compared to the energy difference between the atomic levels. Here we use \mathbf{k} , \mathbf{K} to distinguish z and right-hand polarizations. The energy difference between $F = 1$ and $F = 2$ of $5S_{1/2}$ is about 6.8 GHz, and that between two Rydberg states is also on the GHz scale. This means the phases $(\mathbf{k}_{5S_{1/2}, F=1 \rightarrow 5P_{3/2}} - \mathbf{k}_{5S_{1/2}, F=2 \rightarrow 5P_{3/2}}) \cdot (\mathbf{r}_1 - \mathbf{r}_2)$ and $(\mathbf{K}_{5P_{3/2} \rightarrow n_A S_{1/2}} - \mathbf{K}'_{5P_{3/2} \rightarrow n_B S_{1/2}}) \cdot (\mathbf{r}_1 - \mathbf{r}_2)$ are both on the order of 10^{-3} for nearest-neighbor interaction. Thus we approximately have $\text{Im}H_{23}^{(ab)} = 0$ in this case.

For the other phases, it is useful to set z where the two-dimensional lattice lies as 0, then all the phase terms in Eq. (A54) are defined through the wave vectors of the linearly polarized lasers. For two atoms on sublattice a,

$$\begin{aligned} \phi_{1+} - \phi_{2+} - (\varphi_{1+} - \varphi_{2+}) &= (\mathbf{k}_{5S_{1/2}, F=1 \rightarrow 5P_{1/2}, F=1} - \mathbf{k}_{5S_{1/2}, F=2 \rightarrow 6P_{1/2}, F=1}) \cdot \mathbf{r}_1 - (\mathbf{k}_{5S_{1/2}, F=1 \rightarrow 5P_{1/2}, F=2} - \mathbf{k}_{5S_{1/2}, F=2 \rightarrow 6P_{1/2}, F=2}) \cdot \mathbf{r}_2 \\ &= \mathbf{k}_{5P_{1/2} \rightarrow 6P_{1/2}} \cdot (\mathbf{r}_1 - \mathbf{r}_2) \\ &= k_{5P_{1/2} \rightarrow 6P_{1/2}} |\mathbf{r}_1 - \mathbf{r}_2| \cos \vartheta \equiv \phi \cos \vartheta, \end{aligned} \quad (\text{A55})$$

where the angle ϑ between the wave vector of the linearly polarized laser and the vector $\mathbf{r}_1 - \mathbf{r}_2$ is 0, $m\pi/3$, with m an integer. With $L = 12.798 \mu\text{m}$, here ϕ is about 49.377π , and $(\mu^{(a)}, \mu^{(b)}, t_{\text{NN}}, t_{\text{NN}}^{(aa)}, t_{\text{NN}}^{(bb)}, t_{\text{N}})/2\pi = (-159, -152, 2, 12, 12, -40)\text{Hz}$, and $(U_{\text{NN}}^{(aa)}, U_{\text{NN}}^{(bb)}, U_{\text{N}}^{(ab)})/2\pi = (-9.15, -9.96, 92.7)\text{Hz}$, where t_{N} is the nearest-neighboring hopping and t_{NN} is part of the next-nearest-neighboring hopping that carries no phase.

-
- [1] R. P. Feynman, Simulating physics with computers, *Int. J. Theor. Phys.* **21**, 467 (1982).
- [2] I. Bloch, J. Dalibard, and W. Zwerger, Many-body physics with ultracold gases, *Rev. Mod. Phys.* **80**, 885 (2008).
- [3] I. Bloch, J. Dalibard, and S. Nascimbène, Quantum simulations with ultracold quantum gases, *Nat. Phys.* **8**, 267 (2012).
- [4] I. M. Georgescu, S. Ashhab, and F. Nori, Quantum simulation, *Rev. Mod. Phys.* **86**, 153 (2014).
- [5] K. v. Klitzing, G. Dorda, and M. Pepper, New method for high-accuracy determination of the fine-structure constant based on quantized hall resistance, *Phys. Rev. Lett.* **45**, 494 (1980).
- [6] F. D. M. Haldane, Model for a quantum Hall effect without Landau levels: Condensed-matter realization of the ‘‘parity anomaly’’, *Phys. Rev. Lett.* **61**, 2015 (1988).
- [7] X.-L. Qi, R. Li, J. Zang, and S.-C. Zhang, Inducing a magnetic monopole with topological surface states, *Science* **323**, 1184 (2009).
- [8] M. Z. Hasan and C. L. Kane, Colloquium: Topological insulators, *Rev. Mod. Phys.* **82**, 3045 (2010).
- [9] X.-L. Qi and S.-C. Zhang, Topological insulators and superconductors, *Rev. Mod. Phys.* **83**, 1057 (2011).
- [10] A. Kitaev, Anyons in an exactly solved model and beyond, *Ann. Phys.* **321**, 2 (2006).
- [11] C. Nayak, A. Stern, M. Freedman, and S. Das Sarma, Non-Abelian anyons and topological quantum computation, *Rev. Mod. Phys.* **80**, 1083 (2008).
- [12] N. Goldman, I. Satija, P. Nikolic, A. Bermudez, M. A. Martin-Delgado, M. Lewenstein, and I. B. Spielman, Realistic time-reversal invariant topological insulators with neutral atoms, *Phys. Rev. Lett.* **105**, 255302 (2010).
- [13] X.-J. Liu, K. T. Law, and T. K. Ng, Realization of 2D spin-orbit interaction and exotic topological orders in cold atoms, *Phys. Rev. Lett.* **112**, 086401 (2014).
- [14] A. S. Sørensen, E. Demler, and M. D. Lukin, Fractional quantum Hall states of atoms in optical lattices, *Phys. Rev. Lett.* **94**, 086803 (2005).
- [15] C. Wu, Orbital analogue of the quantum anomalous Hall effect in p -band systems, *Phys. Rev. Lett.* **101**, 186807 (2008).
- [16] T. D. Stanescu, V. Galitski, and S. D. Sarma, Topological states in two-dimensional optical lattices, *Phys. Rev. A* **82**, 013608 (2010).
- [17] E. Tang, J.-W. Mei, and X.-G. Wen, High-temperature fractional quantum Hall states, *Phys. Rev. Lett.* **106**, 236802 (2011).
- [18] K. Sun, Z. Gu, H. Katsura, and S. Das Sarma, Nearly flatbands with nontrivial topology, *Phys. Rev. Lett.* **106**, 236803 (2011).

- [19] Y. F. Wang, Z. C. Gu, C. D. Gong, and D. N. Sheng, Fractional quantum Hall effect of hard-core bosons in topological flat bands, *Phys. Rev. Lett.* **107**, 146803 (2011).
- [20] T. Neupert, L. Santos, C. Chamon, and C. Mudry, Fractional quantum hall states at zero magnetic field, *Phys. Rev. Lett.* **106**, 236804 (2011).
- [21] N. Y. Yao, C. R. Laumann, a. V. Gorshkov, S. D. Bennett, E. Demler, P. Zoller, and M. D. Lukin, Topological flat bands from dipolar spin systems, *Phys. Rev. Lett.* **109**, 266804 (2012).
- [22] N. Y. Yao, A. V. Gorshkov, C. R. Laumann, A. M. Läuchli, J. Ye, and M. D. Lukin, Realizing fractional Chern insulators in dipolar spin systems, *Phys. Rev. Lett.* **110**, 185302 (2013).
- [23] R. Samajdar, W. W. Ho, H. Pichler, M. D. Lukin, and S. Sachdev, Quantum phases of Rydberg atoms on a kagome lattice, *Proc. Natl. Acad. Sci. USA* **118**, e2015785118 (2021).
- [24] A. Browaeys and T. Lahaye, Many-body physics with individually controlled Rydberg atoms, *Nat. Phys.* **16**, 132 (2020).
- [25] C. S. Adams, J. D. Pritchard, and J. P. Shaffer, Rydberg atom quantum technologies, *J. Phys. B: At., Mol. Opt. Phys.* **53**, 012002 (2019).
- [26] X. Wu, X. Liang, Y. Tian, F. Yang, C. Chen, Y. C. Liu, M. K. Tey, and L. You, A concise review of Rydberg atom based quantum computation and quantum simulation, *Chin. Phys. B* **30**, 020305 (2021).
- [27] M. Morgado and S. Whitlock, Quantum simulation and computing with Rydberg-interacting qubits, *AVS Quantum Sci.* **3**, 023501 (2021).
- [28] Y. Li, H. Cai, D.-W. Wang, L. Li, J. Yuan, and W. Li, Many-body chiral edge currents and sliding phases of atomic spin waves in momentum-space lattice, *Phys. Rev. Lett.* **124**, 140401 (2020).
- [29] A. Montorsi, S. Fazzini, and L. Barbiero, Homogeneous and domain-wall topological Haldane conductors with dressed Rydberg atoms, *Phys. Rev. A* **101**, 043618 (2020).
- [30] F. M. Surace, P. P. Mazza, G. Giudici, A. Lerose, A. Gambassi, and M. Dalmonte, Lattice gauge theories and string dynamics in Rydberg atom quantum simulators, *Phys. Rev. X* **10**, 021041 (2020).
- [31] R. Verresen, M. D. Lukin, and A. Vishwanath, Prediction of toric code topological order from Rydberg blockade, *Phys. Rev. X* **11**, 031005 (2021).
- [32] N. E. Myerson-Jain, S. Yan, D. Weld, and C. Xu, Construction of fractal order and phase transition with Rydberg atoms, *Phys. Rev. Lett.* **128**, 017601 (2022).
- [33] K. Li, J.-H. Wang, Y.-B. Yang, and Y. Xu, Symmetry-protected topological phases in a Rydberg glass, *Phys. Rev. Lett.* **127**, 263004 (2021).
- [34] T. F. Gallagher, *Rydberg Atoms* (Cambridge University Press, Cambridge, 1994).
- [35] T. G. Walker and M. Saffman, Consequences of Zeeman degeneracy for the van der Waals blockade between Rydberg atoms, *Phys. Rev. A* **77**, 032723 (2008).
- [36] M. Saffman, T. G. Walker, and K. Mølmer, Quantum information with Rydberg atoms, *Rev. Mod. Phys.* **82**, 2313 (2010).
- [37] X. Wu, F. Yang, S. Yang, K. Mølmer, T. Pohl, M. K. Tey, and L. You, Manipulating synthetic gauge fluxes via multicolor dressing of Rydberg-atom arrays, *Phys. Rev. Res.* **4**, L032046 (2022).
- [38] D. J. Thouless, M. Kohmoto, M. P. Nightingale, and M. Den Nijs, Quantized Hall conductance in a two-dimensional periodic potential, *Phys. Rev. Lett.* **49**, 405 (1982).
- [39] M. Khazali, Discrete-time quantum-walk & Floquet topological insulators via distance-selective Rydberg-interaction, *Quantum* **6**, 664 (2022).
- [40] X.-F. Shi and T. A. B. Kennedy, Simulating magnetic fields in Rydberg-dressed neutral atoms, *Phys. Rev. A* **97**, 033414 (2018).
- [41] X.-F. Shi, Quantum logic and entanglement by neutral Rydberg atoms: Methods and fidelity, *Quantum Sci. Technol.* **7**, 023002 (2022).
- [42] J. Qian, G. Dong, L. Zhou, and W. Zhang, Phase diagram of Rydberg atoms in a nonequilibrium optical lattice, *Phys. Rev. A* **85**, 065401 (2012).
- [43] M. Hönig, D. Muth, D. Petrosyan, and M. Fleischhauer, Steady-state crystallization of Rydberg excitations in an optically driven lattice gas, *Phys. Rev. A* **87**, 023401(R) (2013).
- [44] M. Hoening, W. Abdussalam, M. Fleischhauer, and T. Pohl, Antiferromagnetic long-range order in dissipative Rydberg lattices, *Phys. Rev. A* **90**, 021603(R) (2014).
- [45] A. W. Glaetzle, M. Dalmonte, R. Nath, C. Gross, I. Bloch, and P. Zoller, Designing frustrated quantum magnets with laser-dressed Rydberg atoms, *Phys. Rev. Lett.* **114**, 173002 (2015).
- [46] R. M. W. van Bijnen and T. Pohl, Quantum magnetism and topological ordering via Rydberg dressing near Förster resonances, *Phys. Rev. Lett.* **114**, 243002 (2015).
- [47] M. Kiffner, E. O'Brien, and D. Jaksch, Topological spin models in Rydberg lattices, *Appl. Phys. B* **123**, 46 (2017).
- [48] S. Weber, S. D. Leséleuc, V. Lienhard, D. Barredo, T. Lahaye, A. Browaeys, and H. P. Büchler, Topologically protected edge states in small Rydberg systems, *Quantum Sci. Technol.* **3**, 044001 (2018).
- [49] S. Weber, R. Bai, N. Makki, J. Mögerle, T. Lahaye, A. Browaeys, M. Daghofer, N. Lang, and H. P. Büchler, Experimentally accessible scheme for a fractional chern insulator in Rydberg atoms, *PRX Quantum* **3**, 030302 (2022).
- [50] S. De Leséleuc, V. Lienhard, P. Scholl, D. Barredo, S. Weber, N. Lang, H. P. Büchler, T. Lahaye, and A. Browaeys, Observation of a symmetry-protected topological phase of interacting bosons with Rydberg atoms, *Science* **365**, 775 (2019).
- [51] L. Santos, G. V. Shlyapnikov, P. Zoller, and M. Lewenstein, Bose-Einstein condensation in trapped dipolar gases, *Phys. Rev. Lett.* **85**, 1791 (2000).
- [52] I. Bouchoule and K. Mølmer, Spin squeezing of atoms by the dipole interaction in virtually excited Rydberg states, *Phys. Rev. A* **65**, 041803(R) (2002).
- [53] G. Pupillo, A. Micheli, M. Boninsegni, I. Lesanovsky, and P. Zoller, Strongly correlated gases of Rydberg-dressed atoms: Quantum and classical dynamics, *Phys. Rev. Lett.* **104**, 223002 (2010).
- [54] N. Henkel, R. Nath, and T. Pohl, Three-dimensional roton excitations and supersolid formation in Rydberg-excited Bose-Einstein condensates, *Phys. Rev. Lett.* **104**, 195302 (2010).
- [55] M. Mattioli, M. Dalmonte, W. Lechner, and G. Pupillo, Cluster Luttinger liquids of Rydberg-dressed atoms in optical lattices, *Phys. Rev. Lett.* **111**, 165302 (2013).

- [56] T. Macrì and T. Pohl, Rydberg dressing of atoms in optical lattices, *Phys. Rev. A* **89**, 011402(R) (2014).
- [57] A. W. Glaetzle, M. Dalmonte, R. Nath, I. Rousochatzakis, R. Moessner, and P. Zoller, Quantum spin ice and dimer models with Rydberg atoms, *Phys. Rev. X* **4**, 041037 (2014).
- [58] I.-D. Potirniche, A. C. Potter, M. Schleier-Smith, A. Vishwanath, and N. Y. Yao, Floquet symmetry-protected topological phases in cold-atom systems, *Phys. Rev. Lett.* **119**, 123601 (2017).
- [59] K. Afrousheh, P. Bohlouli-Zanjani, D. Vagale, A. Mugford, M. Fedorov, and J. D. D. Martin, Spectroscopic observation of resonant electric dipole-dipole interactions between cold Rydberg atoms, *Phys. Rev. Lett.* **93**, 233001 (2004).
- [60] G. Günter, H. Schempp, M. Robert-de Saint-Vincent, V. Gavryusev, S. Helmrich, C. S. Hofmann, S. Whitlock, and M. Weidemüller, Observing the dynamics of dipole-mediated energy transport by interaction-enhanced imaging, *Science* **342**, 954 (2013).
- [61] S. De Léséleuc, D. Barredo, V. Lienhard, A. Browaeys, and T. Lahaye, Optical control of the resonant dipole-dipole interaction between Rydberg atoms, *Phys. Rev. Lett.* **119**, 053202 (2017).
- [62] L. Isenhower, E. Urban, X. L. Zhang, A. T. Gill, T. Henage, T. A. Johnson, T. G. Walker, and M. Saffman, Demonstration of a neutral atom controlled-not quantum gate, *Phys. Rev. Lett.* **104**, 010503 (2010).
- [63] Q. Liu, C.-X. Liu, C. Xu, X.-L. Qi, and S.-C. Zhang, Magnetic impurities on the surface of a topological insulator, *Phys. Rev. Lett.* **102**, 156603 (2009).
- [64] J. Q. You, X.-F. Shi, X. Hu, and F. Nori, Quantum emulation of a spin system with topologically protected ground states using superconducting quantum circuits, *Phys. Rev. B* **81**, 014505 (2010).
- [65] C. Laflamme, M. a. Baranov, P. Zoller, and C. V. Kraus, Hybrid topological quantum computation with Majorana fermions: A cold-atom setup, *Phys. Rev. A* **89**, 022319 (2014).
- [66] X.-F. Shi, F. Bariani, and T. A. B. Kennedy, Entanglement of neutral-atom chains by spin-exchange Rydberg interaction, *Phys. Rev. A* **90**, 062327 (2014).
- [67] I. Shavitt and L. T. Redmon, Quasidegenerate perturbation theories. A canonical van Vleck formalism and its relationship to other approaches, *J. Chem. Phys.* **73**, 5711 (1980).
- [68] R. Winkler, *Spin-Orbit Coupling Effects in Two-Dimensional Electron and Hole Systems*, Springer Tracts in Modern Physics (Springer-Verlag, Berlin, 2003).
- [69] J. E. Sansonetti, Wavelengths, transition probabilities, and energy levels for the spectra of rubidium (Rb I through Rb XXXVII), *J. Phys. Chem. Ref. Data* **35**, 301 (2006).
- [70] D. Peter, N. Y. Yao, N. Lang, S. D. Huber, M. D. Lukin, and H. P. Buchler, Topological bands with a Chern number $C = 2$ by dipolar exchange interactions, *Phys. Rev. A* **91**, 053617 (2015).
- [71] M. F. Maghrebi, N. Y. Yao, M. Hafezi, T. Pohl, O. Firstenberg, and A. V. Gorshkov, Fractional quantum Hall states of Rydberg polaritons, *Phys. Rev. A* **91**, 033838 (2015).
- [72] M. Kwon, M. F. Ebert, T. G. Walker, and M. Saffman, Parallel low-loss measurement of multiple atomic qubits, *Phys. Rev. Lett.* **119**, 180504 (2017).
- [73] Y. Wang, A. Kumar, T.-Y. Wu, and D. S. Weiss, Single-qubit gates based on targeted phase shifts in a 3D neutral atom array, *Science* **352**, 1562 (2016).
- [74] T. Boulier, E. Magnan, C. Bracamontes, J. Maslek, E. A. Goldschmidt, J. T. Young, A. V. Gorshkov, S. L. Rolston, and J. V. Porto, Spontaneous avalanche dephasing in large Rydberg ensembles, *Phys. Rev. A* **96**, 053409 (2017).
- [75] L. Festa, N. Lorenz, L.-M. Steinert, Z. Chen, P. Osterholz, R. Eberhard, and C. Gross, Blackbody-radiation-induced facilitated excitation of Rydberg atoms in optical tweezers, *Phys. Rev. A* **105**, 013109 (2022).
- [76] W.-W. Luo, A.-L. He, Y. Zhou, Y.-F. Wang, and C.-D. Gong, Quantum phase transitions in a $\nu = 1/2$ bosonic fractional Chern insulator, *Phys. Rev. B* **102**, 155120 (2020).
- [77] R. B. Laughlin, Quantized Hall conductivity in two dimensions, *Phys. Rev. B* **23**, 5632 (1981).
- [78] A. Alexandradinata, T. L. Hughes, and B. A. Bernevig, Trace index and spectral flow in the entanglement spectrum of topological insulators, *Phys. Rev. B* **84**, 195103 (2011).
- [79] B. Andrews, M. Mohan, and T. Neupert, Abelian topological order of $\nu = 2/5$ and $3/7$ fractional quantum Hall states in lattice models, *Phys. Rev. B* **103**, 075132 (2021).
- [80] J. Hauschild and F. Pollmann, Efficient numerical simulations with tensor networks: Tensor Network Python (TeNPy), *SciPost Phys. Lect. Notes* **5** (2018).
- [81] E. Brion, L. H. Pedersen, and K. Mølmer, Adiabatic elimination in a lambda system, *J. Phys. A: Math. Theor.* **40**, 1033 (2007).